

72320 Roversystemtechnik
Summer Semester 2021

**Phase 0/A-Study of a Rover Mission on the Surface
of the Jupiter moon Europa**

INSPIRE

**IN-situ Sampling and Primal Investigation
Rover on Europa**



Denis Acker
Daniel Bölke
Korbinian Kasper
Christian Korn
Nicolas Probst
Saskia Süitterlin

Supervisors:
Moritz Nitz M.Sc.
Patrick Winterhalder M.Sc.

University of Stuttgart
Institute of Space Systems
Prof. Dr. Sabine Klinkner
18.07.2021

Symbols

Symbol	Definition	Unit
a	Constant for the Geometry of a Porous Media	nm
A	Wheel Ground Contact Area	m
b_w	Wheel Width	m
c	Coefficient of Soil Cohesion	Pa
$C_{\text{batt},\text{req}}$	Total Required Battery Capacity	Wh
$C_{\text{batt},\text{nom}}$	Battery Nominal Capacity	Wh
C_{cell}	Cell Voltage	V
CON_*	Heat conductance of concerning component	$\frac{W}{K}$
C_{rr}	Rolling Resistance Coefficient	-
d	Wheel Distance Vertical	m
d_w	Wheel Diameter	m
DoD	Depth of Discharge	%
DP	Drawbar Pull	N
G_R	Antenna Gain Rover	dB
H	Soil Thrust	N
h_{ice}	Ice Crust Surface Thickness on Europa	m
k_c	Sinkage Modulus	$\frac{kN}{m^{n+2}}$
k_ϕ	Soil Friction Angle Sinkage Modulus	$\frac{kN}{m^{n+3}}$
L_1	Line Loss	dB
L_p	Polarisation Loss	dB
L_a	Atmospheric Loss	dB
L_{11}	Degradation and Implementation Loss	dB
l_w	Wheel Ground Contact Length	m
l	Wheel Distance Length	m
R_t	Heat resistance	$\frac{K}{W}$
T_{surface}	Surface Temperature on Europa	K
M	Number of Cells in Parallel	-
MMP	Mean Maximum Pressure	kPa
m_{RTG}	RTG Mass	kg
m_w	Weight per Wheel	kg
n	Soil Deformation Exponent	-
N	Number of Cells in Series	-
P	Wheel Electrical Power	W
P_{el}	RTG Electrical Power	W_{el}
$P_{\text{el},\text{req}}$	Required Electrical Power	W_{el}
P_{mode}	Demanded Electrical Power per Mode	W_{el}

SYMBOLS

P_R	Transmitter Output Power Rover	W
\dot{Q}	Heat flow	W
S_0	Solar constant	$\frac{W}{m^2}$
R	Data Rate	kbps
R_b	Bulldozing Resistance	N
R_c	Compaction Resistance	N
R_g	Gravitational Resistance	N
R_r	Rolling Resistance	N
R_{total}	Total Resistance	N
S	Radiation Surface	m^2
T_s	Effective Noise Temperature	K
t_e	Mode Duration	s
v	Velocity	$\frac{m}{s}$
W	Normal Force	N
W_w	Normal Force per Wheel	N
z	Sinking Depth	m
α	Absorptivity	-
α_{BOL}	BOL Specific Power	$\frac{W_{el}}{kg}$
δ	Wheel Deflection	m
δ_R	Ecliptic latitude of the rover on Europa	deg
ϵ	Emissivity	-
η_{LiIon}	Efficiency of LiIon Cells	-
λ	Heat conductivity	$\frac{W}{mK}$
λ_R	Ecliptic longitude of the rover on Europa	deg
Φ	Friction Angle	deg
φ	View factor	-
ρ_E	Albedo of Europa	-
ρ_{ice}	Inner Encoder Ring Diameter	$\frac{kg}{m^3}$
σ_b	Stefan-Boltzmann constant	$\frac{W}{m^2 K^4}$
θ	Slope Angle	deg
τ	Torque	Nm

Abbreviations

2D	Two Dimensional
3D	Three Dimensional
APXS	Alpha Particle X-Ray Spectrometer
BER	Bit Error Rate
BLDC	Brushless Direct Current
BOL	Begin of Life
BOM	Begin of Mission
COMM	Communications
COTS	Commercial of the Shelf
C&DH	Command & Data Handling
CPU	Core Processing Unit
DoD	Depth of Discharge
eMMRTG	Enhanced Multi Mission Radioisotope Thermoelectric Generator
eSMMRTG	Enhanced and Scaled Multi Mission Radioisotope Thermoelectric Generator (3kg)
EOM	End of Mission
EPS	Electrical Power System
ESA	European Space Agency
FEC	Forward Error Correction
GPR	Ground Penetrating Radar
HGA	High Gain Antenna
HPC	High Priority Commands
IRS	Institute of space Systems at the University of Stuttgart
IMU	Inertial Measurement Unit
INSPIRE	IN-situ Sampling and Primal Investigation Rover on Europa
JUICE	Jupiter Icy Moons Explorer
LGA	Low Gain Antenna
MP	Mobility Package
NASA	National Aeronautics and Space Administration
OBC	On-Board Computer
PCDU	Power Control and Distribution Unit
PCU	Power Control Unit
PDU	Power Distribution and Control Unit
RHU	Radioisotope Heater Unit
RTG	Radioisotope Thermoelectric Generator
S/C	Spacecraft
SBC	Single Board Computer
SPENVIS	SPace ENVironment Information System
TID	Total Ionizing Dose
TRIPLE	Technologies for Rapid Ice Penetration and Subglacial Lake Exploration
TRL	Technology Readiness Level

Contents

Symbols	I
Abbreviations	III
List of Figures	VI
List of Tables	VII
1 The Mission	1
2 Payload	2
2.1 Ground RADAR	2
2.2 Ice Core Drill	2
2.3 APXS Analyser	2
2.4 Stereovision Camera / Observation / Perception	3
2.5 RadHard Solar Arrays	3
3 Operation	4
3.1 Scientific Output	4
3.2 Rover System Modes	5
4 Subsystems	6
4.1 Structure and Mechanisms	6
4.1.1 Storage Configuration and Rover Deployment	6
4.1.2 Exploration Configuration	7
4.1.3 Static Analysis	7
4.1.4 Mass Budget	8
4.2 Locomotion	8
4.2.1 Design Drivers for Rover Classification	8
4.2.2 System Parameters	8
4.2.3 Deployment mechanism	11
4.3 Electrical Power System	11
4.3.1 EPS Budget and Overview	12
4.3.2 Energy Source	12
4.3.3 Energy Storage	13
4.3.4 EPS Power Control and Distribution	14
4.4 Communications and Command & Data-Handling	14
4.4.1 Operational Concept	14
4.4.2 Communication System	14
4.4.3 Command & Data Handling	15
4.5 Thermal Control System	16
4.5.1 Concepts	16
4.5.2 Thermal Network	17
4.5.3 Analysis	18
4.5.4 Results	18
4.6 Radiation	19
4.6.1 Radiation Protection	19
4.6.2 Components	19

4.6.3	Improvements	20
4.6.4	Conclusion	20
5	Outlook & Risk Assessment	21
5.1	Risk Assessment	21
5.2	Outlook	22
	Bibliography	23
	Appendix	26
A	Operation	26
B	Structure and Mechanism	27
C	Locomotion	29
C.1	Locomotion Design Drivers	29
D	Electrical Power System	32
E	Communications	34
E.1	Link Budget	34
E.2	Mission Data Output	38
F	Thermal Controls System	39
F.1	Results	39
F.2	Heat energy eqilibrium	39
F.3	Heat conductance	42
F.4	Heat switch	46
F.5	Rover absorptivity	47
F.6	Input Values	48
G	Radiation	51
G.1	Jupiters Radiation Environment	51
G.2	Radiation Exposures	52
G.3	Improvements	53
H	Digital Appendix	55

List of Figures

2.1	Left: Ice Core Drill in stowed configuration, Right: Ice Core Drill in drilling configuration	3
2.2	INSPIRE's Surface Observation System including CamHead and Hazcams + Ground Radar	3
3.1	Preliminary Mission Timeline for INSPIRE.	4
3.2	Timeline of a mission day during phase 4	4
4.1	Geometrical Data of Storage Configuration inside the lander.	6
4.2	Results of the investigation into the tilting behaviour of the INSPIRE Rover System.	7
4.3	Wheel sinkage z as a function of the slope angle θ of each configuration with different soil parameters, referred to Table C.1. More information about the calculation can be found in Table H.1.	9
4.4	Comparison of the rover's soil thrust versus the motion resistance to exceed, each for the soil parameters of snow in Sweden and heavy clay, referenced to Table C.1. Additional information about the calculation can be found in Table H.1.	10
4.5	Functional Flow Chart Diagram for the EPS Subsystem.	11
4.6	Functional Flow Chart Diagram for the EPS Subsystem.	12
4.7	Carbon-based thermal strap <i>LyNX®</i>	16
4.8	Bi-metallic heat switch [37].	17
4.9	Change of the heat switch conductivity R_t over the mean temperature T_M	17
4.10	Thermal network of the rover.	18
4.11	Overview of TIDs within different compartments within the rover.	20
5.1	The INSPIRE rover system in it's configurations	22
C.1	Geometric dimensions for the locomotion system.	29
C.2	Parameters for the mean maximum pressure for a wheeled rover.	30
C.3	Mean maximum pressure plotted over the deflection δ . The maximum value of 40 kPa is only exceeded for very small values of δ	31
D.1	Holistic Power Budget of INPSIRE.	33
E.1	Bit Error Rate for different FEC codes	35
F.1	Conductance characteristic of heat switch diveded in sections.	47
F.2	Bi-metallic heat switch [37].	48
F.3	Digitalised [34] and calculated heat conduction in comparison.	49
G.1	Average trapped proton and electron fluxes on an orbit around earth at 25,000 km, through the outer Van Allen radiation belt, and on Europa's orbit around Jupiter.	51
G.2	TID of aluminium, titanium, and the optimised radiation structure shown in Table 4.6 with a weight target of all three structures of 0.5 g/cm^2 over 30 days of exposure on Europa.	52
G.3	TID for different compartments as seen in Figure 4.11. The E-Bay is shielded by 4 mm aluminium, 0.415 mm lead, and 0.033 mm iron; the camera compartment by 2 mm aluminium, 0.415 mm lead, and 0.033 mm iron; the chassis by 2 mm aluminium; the electric motors by 1 mm aluminium.	52
G.4	TID with 4 mm Al shielding over a mission duration of 30 days	54
G.5	TID with 4 mm Al shielding and 1 cm of Water over a mission duration of 30 days	54

List of Tables

2.1 GPR antenna properties [8].	2
3.1 Expected scientific data output of the INSPIRE mission.	5
4.1 Fundamental rover design and the respective design drivers.	8
4.2 Configurations for rover classification respective to the wheel width bw , wheel diameter d_w and weight per wheel m_w	9
4.3 Parameters for the scaled eSMMRTG based on the eMMRTG.	13
4.4 Power consumption mode used as design case for the battery sizing.	14
4.5 Key criteria of selected communication components (data-sheets Table H.1).	15
4.6 Optimal shield structure for an Jupiter mission. [41]	19
5.1 Subsystem TRL for risk assessment	21
A.1 Collection of Rover System Modes.	26
B.1 INSPIRE mass budget.	27
B.2 INSPIRE chassis mass budget.	28
C.1 Soil parameters for both soils considered: heav clay as hard equivalent for ice values and snow in Sweden [22].	29
C.2 Various wheel dimensions respective to the weight. Highlighted fields in red are not considered further for system design due to the limit of 200 g weight per wheel.	30
C.3 Calculated torque and power of the configuration 6 in respect to the slope angle and velocity.	31
D.1 INSPIRE battery parameters.	32
E.1 Transmission link parameters.	34
E.2 Complete link budget for Rover to Lander transmission.	36
E.3 Complete link budget for Lander to Rover (L2R) transmission.	37
E.4 Comparison of transmission times per image (message frame bits included)	38
E.5 Transmission time and total data output per mission day	38
F.1 Temperature results in K of thermal analysis, <i>with out</i> margin	39
F.2 Temperature results in K of thermal analysis, <i>with</i> margin	39
F.3 Definition of heat conductance C between the nodes according to Figure 4.10.	42
F.4 Definition of heat conductance $CON = \frac{1}{R}$ between the nodes according to Figure 4.10.	43
F.5 Definition of heat conductance $CON = \frac{1}{R}$ between the nodes according to Figure 4.10.	44
F.6 Definition of heat conductance $CON = \frac{1}{R}$ between the nodes according to Figure 4.10.	45
F.7 Definition of heat conductance $CON = \frac{1}{R}$ between the nodes according to Figure 4.10.	46
F.8 Toggle temperature and amount of bi-metallic heat switch.	46
F.9 Sections and range of the switch characteristic.	47
F.10 Temperatur limits of the rover components.	48
F.11 Dimensions of the thermal straps <i>LyNX®</i>	49
F.12 Minimum and maximum of surface emissivity and absorptivity values [38].	50
F.13 Heat conductivity in $\frac{W}{mK}$	50
F.14 Radiation surface and finishing of components.	50
G.1 Used components and the respective radiation tolerance and location	53
H.1 Digital Appendix	55

Chapter 1

The Mission

During the observation of Jupiter, the Galileo spacecraft performed flybys of the Jupiter moons [1]. The scientist gathered data from Europa, which supported the evidence of a thick icy surface. The possibility of liquid water underneath led astrobiologists to the assumption that extraterrestrial life could exist on Europa [2]. That is why Europa is - beside Mars - an interesting object of research.

Therefore, ESA will launch the *JUICE* orbiter in 2022 to investigate Europa in more detail [3]. Nevertheless, also NASA is developing the *Europa Clipper* to get detailed information. Additionally, they plan a lander for Europa to bring scientific instruments onto the surface [4, 5].

Under the leadership of Prof. Dr.-Ing. Klinkner, the Institute of Space Systems, started within a seminar a feasibility study about a rover system to explore Europa surface, which shall be part of the *TRIPLE* mission. This challenge was given to five student teams to develop concepts, construct preliminary designs, perform analysis and make evaluations to meet the mission objectives and fit the mandatory requirements.

This report contains the results of the Phase 0/A study of the rover system IN-SITU SAMPLING AND PRIMAL INVESTIGATION ROVER ON EUROPA (INSPIRE).

Chapter 2

Payload

Without a Payload, there is no mission. The payload itself is significant for the design and layout of a rover system. It gives meaning and purpose to the system. The components of the payload carried along are examined in detail below.

2.1 Ground RADAR

The Ground Radars main task is the identification of suitable drilling sites. Additionally, every radar campaign will contribute to further understanding of the ground composition on Europa. Due to its small dimensions, the CRUX GPR is selected. The system is tested for lunar application at 800 MHz, resulting in a resolution of 15 cm and a penetration depth of 5 m [6]. The INSPIRE mission makes use of a 1.5 GHz frequency to increase the resolution. Reduced penetration depths are acceptable since the depth of interest for the ice core sampling is 10 cm (see Section 2.2).

Additionally, high frequencies lead to a compact antenna design which is beneficial to the INSPIRE mission due to weight constraints. A custom patch antenna with the properties in Table 2.1 is proposed [7, 8].

Table 2.1: GPR antenna properties [8].

Substrate ε_r	Width	Length	Height	Mass
20	30 mm	20 mm	2 mm	2.73 g

2.2 Ice Core Drill

The Ice Core Drill is an in-house development based on drills from Honeybee Robotics [9, 10] and the drill from Philae [11]. The drill bit is made out of titanium to ensure that it does not deform or even breakthrough during the drilling process. The ice core sample that can be obtained has a length of 100 mm and a diameter of 10 mm. In order to save space, the drill is retracted while driving and will be extended for drilling, which is illustrated in the following Figure 2.1. After finishing the drill process, the drill retracts and the sample can be pushed out with the help of a piston, and meanwhile, it can be analysed by the APXS sensor. When the sample has left the drill body, and the analysis is completed, the rover can switch back to locomotion mode and look for a new place to drill. As soon as a new drilling process starts, the previously taken sample falls to the ground to make room for a new one.

2.3 APXS Analyser

The Alpha Particle X-Ray Spectrometer is an analyser that has been used in many explorer missions like the Philae lander or the Mars rover Curiosity [12, 13]. The spectrometer uses alpha particles as well as X-rays to identify the sort of atom inside a probe. The main advantage is the small mass and the low power it needs during the operation. As a result of the relatively

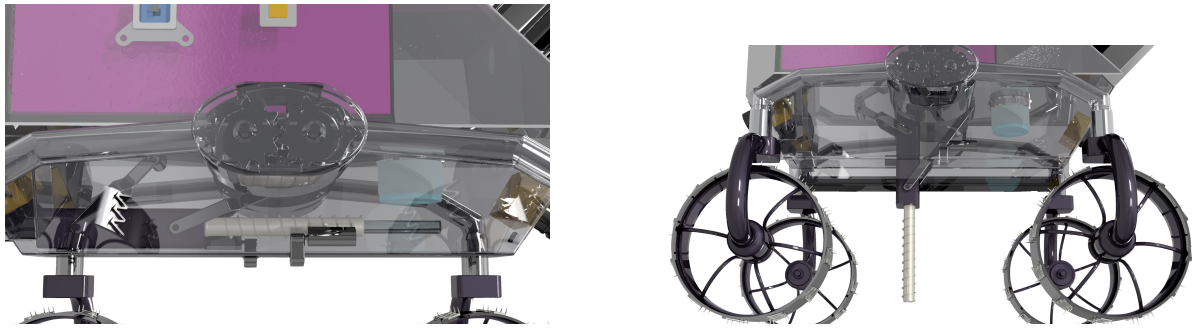


Figure 2.1: Left: Ice Core Drill in stowed configuration, Right: Ice Core Drill in drilling configuration

thin ice core samples, one-third of APXS sources and detectors will be used. Therefore, the mass and power consumption were downsized by one-third because the electronics keep the same and can't be reduced.

2.4 Stereovision Camera / Observation / Perception

The INSPIRE rover is equipped with five individual cameras. Two are used as stereo vision cameras on a height-adjustable and rotatable telescope arm on the front side of the rover. This is used to capture a detailed 3D model of the environment with which sizes and distances can be estimated. The remaining three cameras are used as hazcams which are necessary to obtain data regarding the nearby environment. All cameras are equipped with radiation-hardened lenses to prevent browning of the lenses. Additional information is provided in Table H.1. The main tasks of the camera system are the provision of scientific data and navigation-related data.



Figure 2.2: INSPIRE's Surface Observation System including CamHead and Hazcams + Ground Radar

2.5 RadHard Solar Arrays

As a secondary mission goal for INSPIRE, a cooperation with the European project RadHard, led by the German solar array manufacturer Azure Space is intended. The company currently develops a new generation of 4 junction solar cells with up to 35 % efficiency. However, the main feature of the new solar arrays is their radiation hardness which will be the highest radiation hardness of > 3 % after $1E15 \text{ cm}^{-2}$ 1 MeV electron irradiation. The Jupiter environment, with its extreme radiation, represents a suitable destination for a technology demonstration mission. Therefore INSPIRE will be equipped with 10 RadHard solar cells with a total surface area of 0.0310 m^2 as a technology demonstration [14].

Chapter 3

Operation

For the Phase 0/A study of the INSPIRE Mission five basic mission phases have been defined. The nominal mission will last 30 Earth days which is equal to 8.47 Europa days [15]. Furthermore, a sixth optional mission phase after the nominal mission lifetime has been established which will be conducted if the rover is still operational after its nominal lifetime.

- **Phase 0:** Launch and Flight Phase
- **Phase 1:** Entry, Descent and Landing Phase
- **Phase 2:** Deployment Phase
- **Phase 3:** Egress, Commissioning and Early Operation Phase
- **Phase 4:** Mission Operation Phase
- **(Phase 5:** Exceeding Mission Operation Phase)



Figure 3.1: Preliminary Mission Timeline for INSPIRE.

Based on these mission phases some preliminary rover system modes as well as a basic mission timeline were concluded.

3.1 Scientific Output

Optical reference systems for path planning limit operation of the rover to an average of 45 h of sunlight out of 85 h in a Europa day [15]. Figure 3.2 depicts a breakdown of possible continuous execution times in a mission day based on the power budget. Nevertheless, the given order can be changed and execution times can be adapted to fit the mission requirements.

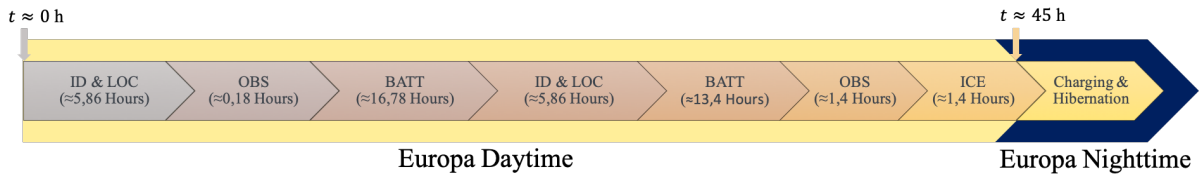


Figure 3.2: Timeline of a mission day during phase 4

Locomotion phases consist of a sequence of mobility packages (MP). Each MP is built up of 5 min path planning and 10 s driving. Path planning time is estimated based on the limited processor speed (see Subsection 4.4.3).

Within the 6 h of a single locomotion phase, a distance of 68 m is covered, resulting in a maximum distance of 1.15 km for the nominal mission.

With respect to the payloads of the INSPIRE mission described in Chapter 2, the scientific return for phase 4 will consist of the data in Table 3.1.

The total data output can be increased further in the case of a sufficient power margin during operation.

Table 3.1: Expected scientific data output of the INSPIRE mission.

Payload	Data Output	Data Output
GPR	raw radar measurements	40
Cameras	grayscale images with optional 3D mapping	>3570 images
Sample Analyser	raw mineral analysis of ice core	10 - 12 samples
Solar Cells	performance data	continuous

3.2 Rover System Modes

For this case study several rover system modes were defined. All ten modes are listed in Table A.1. They are separated into two groups. The design critical modes are displayed in white and are defined as system modes. System modes prove to be crucial for system design. Non-design critical modes extend from the rover storage and launch until the surface deployment of the rover. Their influence on the rover design depends heavily on the final design of the Europa lander. Therefore, a clear definition of non-critical modes is not possible in the course of this Phase 0/A study. However, the respective considerations, preferences and options have been briefly described in the mode descriptions. It is important to note that INSPIRE's goal is to provide a flexible rover design with as few hard requirements as possible for the lander. Therefore, many aspects of the rover, as well as the none design critical modes, will need to be further defined in later phases of the project in close consultation with the customer. For example, the exact interfaces between rover and lander should be defined in more detail. Depending on the subsequently chosen interfaces, many possibilities may arise in the corresponding rover system modes. With a correspondent interface, for example, the excess electrical and thermal energy of the RTG, which is already active during the flight, could be used to supply the lander system with heat and power. A corresponding interface could also enable the transmission of health checks from INSPIRE.

The deployment phase will strongly depend on the final design of the lander, INSPIRE's position within the lander and also the possibilities that the lander provides to INSPIRE. Possible deployment strategies would be the following:

- **Option 1:** If INSPIRE is on ground level: Release from storage box through spring mechanism or actuators. Rover storage configuration allows rolling and possible motorised actuation
- **Option 2:** If INSPIRE is above ground level: Similar as Option 1 but an additional ramp and ramp deployment would be required.
- **Option 3:** INSPIRE will be deployed through the landers robotic arm if it is capable of lifting its mass.

Chapter 4

Subsystems

In this chapter, the individual subsystems of the rover system will be discussed in more detail.

4.1 Structure and Mechanisms

The Structure and Mechanisms subsystem mainly deals with the accommodation of the payloads and all necessary components for the operation of the rover system. This also includes the mechanisms that are necessary for the rover system to ensure its functionality. In the design process, the material aluminum 7075 [16] is used because it saves weight in relation to the size of the rover and the complexity in relation to other materials.

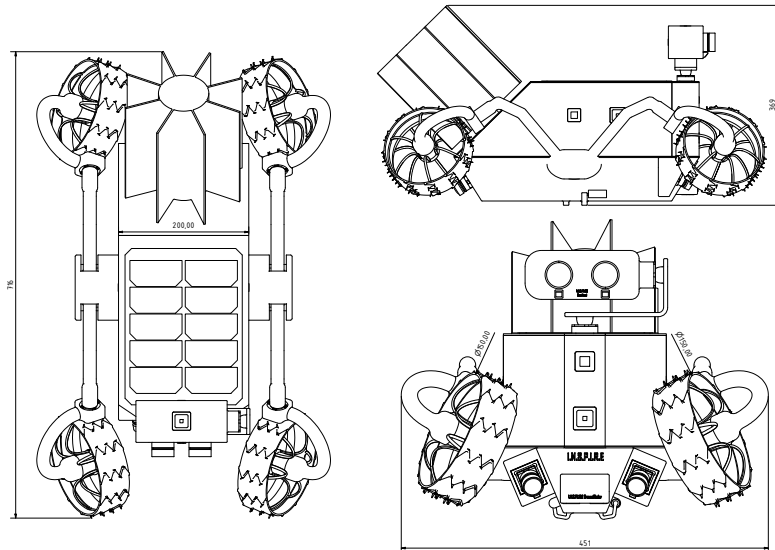


Figure 4.1: Geometrical Data of Storage Configuration inside the lander.

4.1.1 Storage Configuration and Rover Deployment

The main characteristics of the rover chassis design of INSPIRE focuses on compact storage geometry and low mass. The geometry data in storage configuration is shown in Figure 4.1. The storage volume that is required is 131 l. For the rover deployment, option 1 and option 2 described in Section 3.2 are most suitable, but a ramp is more likely and involves a more complex design. Consequently, for this conservative feasibility study option 2 is used and the mechanism is briefly described in the following.

The rover is stowed in the lander as in Figure 5.1a and must first place its wheels parallel to the chassis. Then the bogies are rotated by at least 15 degrees so that the Chassis lifts slightly from the lander. As soon as this has happened, a mechanism is triggered which unfolds the ramp. Now INSPIRE can carefully roll out of the lander until it finally reaches the surface of Europa.

4.1.2 Exploration Configuration

When the deployment is successfully, INSPIRE has to switch from storage to exploration configuration. This will be possible with a cogwheel mechanism which will be operated by two motors. When the wheel forks are horizontal to the ground, the rover is ready for its journey. In order to maintain the rover stability while driving on rough terrain an averaging differential mechanism is needed. This will be achieved by a planetary gear with a transmission ration of 1:1. One bogie then will execute a counter movement due to the tilt of the other bogie. (Figure 5.1b)

4.1.3 Static Analysis

Part of the design process was to examine the stability of the rover. In order to determine the maximum possible gradients, an adjustable gradient was simulated using the CAD model, on which the rover system was then placed. The results of this investigation can be seen in Figure 4.2. As shown, significantly higher angles are possible if the center of gravity of the rover is offset by the expansion mechanism. Due to the symmetrical design and the central position of the center of gravity, investigations were only carried out for one half of the chassis. The maximum possible angles are therefore assumed to be identical on both sides.

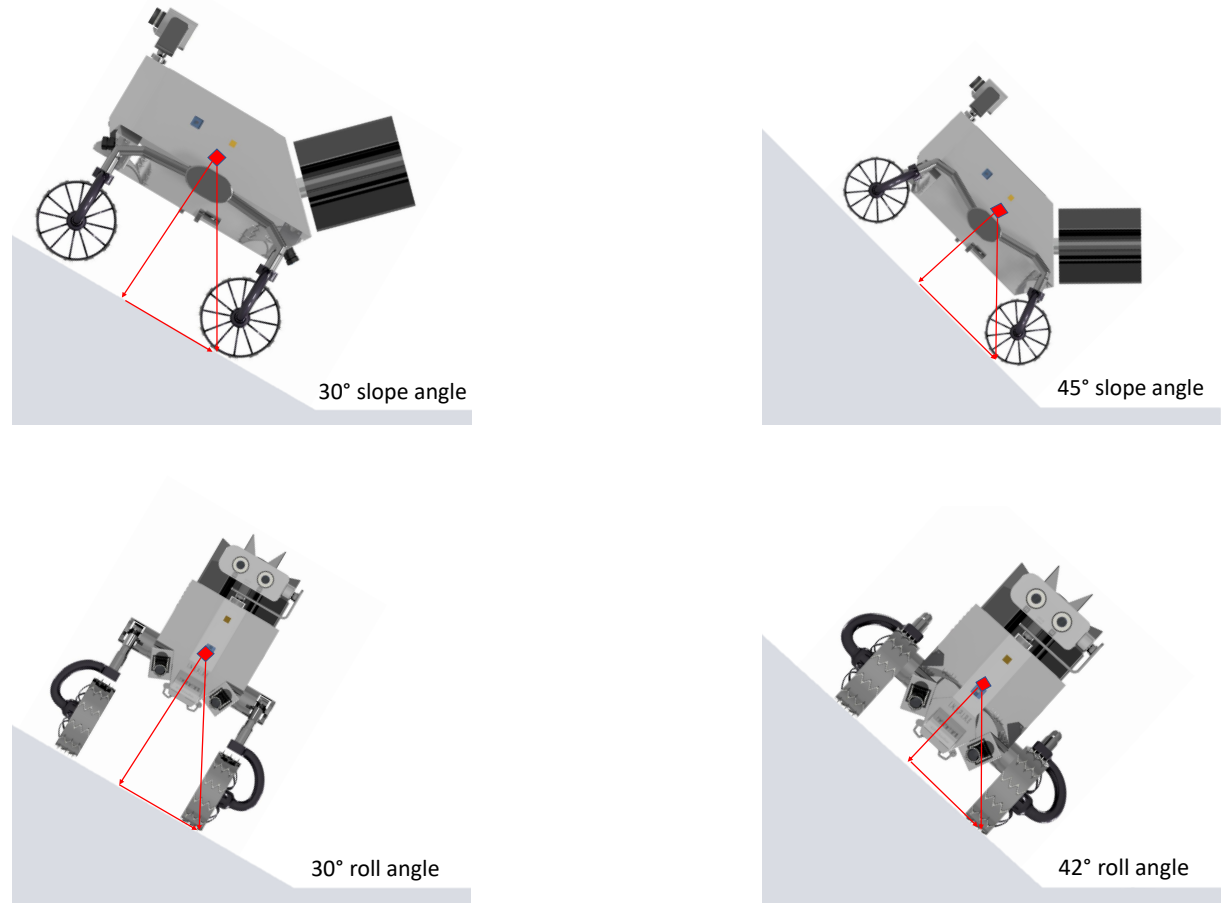


Figure 4.2: Results of the investigation into the tilting behaviour of the INSPIRE Rover System.

4.1.4 Mass Budget

Due to the strict mass restriction, it is quite difficult to find a suitable concept that is both, light and space-saving. In order to make the design process of INSPIRE more effective, a specially selected preferred maximum mass of the chassis with the mechanisms of 5 kg was chosen. A table with all components of the INSPIRE Rover system is shown in Table B.1.

4.2 Locomotion

The locomotion subsystem deals with the aspect of how the rover moves and the technical design, including the selection of components such as motors or gears. Before the components can be determined, however, it is necessary to consider certain parameters and design drivers. These will be introduced in the following, and the decisions or estimations concerning the rover will be presented.

4.2.1 Design Drivers for Rover Classification

The fundamental rover design can be described by the wheel formula 4x4x4, based on a tradeoff, listed in Table H.1. A more detailed design and the main criteria related to this are summarised in Table 4.1.

Table 4.1: Fundamental rover design and the respective design drivers.

Wheeled System	4-Wheels
One of the most common types of platform - high level of experience - high TRL	Compared to 2-wheels: - stability can be ensured → important for drilling - <i>MMP</i> decreases
Compared to other systems: - analysis quite straightforward - simplification → one of the most critical design drivers	Compared to 6-wheels: - less complex → simplification - mass can be reduced
All-Wheel Drive	All-Wheel Actuation
- traction can be increased - increase of <i>DP</i> and the slope angle θ	- reduces the risk of slippage on ice

Furthermore, the normal force on Europa can be calculated to $W = m_{\text{total}} \cdot g_{\text{Europa}} = 39.45 \text{ N}$ [17]. Since each wheel is individually driven and controllable, the parameters in the following are designed for one wheel; the normal force per wheel is correspondingly $W_w = 9.8625 \text{ N}$.

4.2.2 System Parameters

Regarding techniques of rover movement, it is crucial to consider the local conditions in which the rover will be operating. The surface of Europa can be assumed to be mainly covered by ice. However, since there are also geysers that transport water to the surface, surface areas may be covered by snow [18]. Though Europa's surface temperature does not exceed 130 K, rather icy, hard-packed snow can be assumed. For this study, a conservative design of the rover is considered, with soil parameters of snow in Sweden as well as heavy clay as a substitute for a hard ice surface; both are listed in Table C.1. Furthermore, the parameters depend on the width and diameter of the wheels of the rover. Therefore, several sizes dependent on the respective weight were selected and a limit per wheel was set to 200 g, illustrated in Table C.2. This constraint results in 6 configurations considered for the Rover system design, listed in Table 4.2. All necessary geometrical dimensions of the locomotion system are shown in Figure C.1.

Table 4.2: Configurations for rover classification respective to the wheel width b_w , wheel diameter d_w and weight per wheel m_w .

Configuration	b_w / m	Diameter d_w / m	Weight m_w / kg	Configuration	b_w / m	Diameter d_w / m	Weight m_w / kg
1	0.05	0.1	0.127	4	0.05	0.125	0.154
2	0.06	0.1	0.153	5	0.05	0.125	0.185
3	0.07	0.1	0.178	6	0.05	0.15	0.185

Trafficability Configuration

The ability of traffic depends on the soil parameters as well as on the geometric dimensions of the wheels. The sinking depth z for each wheel of the rover can be determined to [19]:

$$z = \left(\frac{3W_w \cos \theta}{(3-n)(k_c + b_w k_\phi) \sqrt{d_w}} \right)^{\frac{2}{2n+1}}. \quad (4.1)$$

As shown in Figure 4.3, the sinking depth z depends not only on the geometric conditions and soil parameters but also on the slope angle θ . Therefore, z can be determined for both soils with respect to θ as plotted in Figure 4.3. However, it can be assumed that for the expected soil, the following applies: $z_{\text{Heavy Clay}} \leq z_{\text{Europa}} \leq z_{\text{Snow}}$.

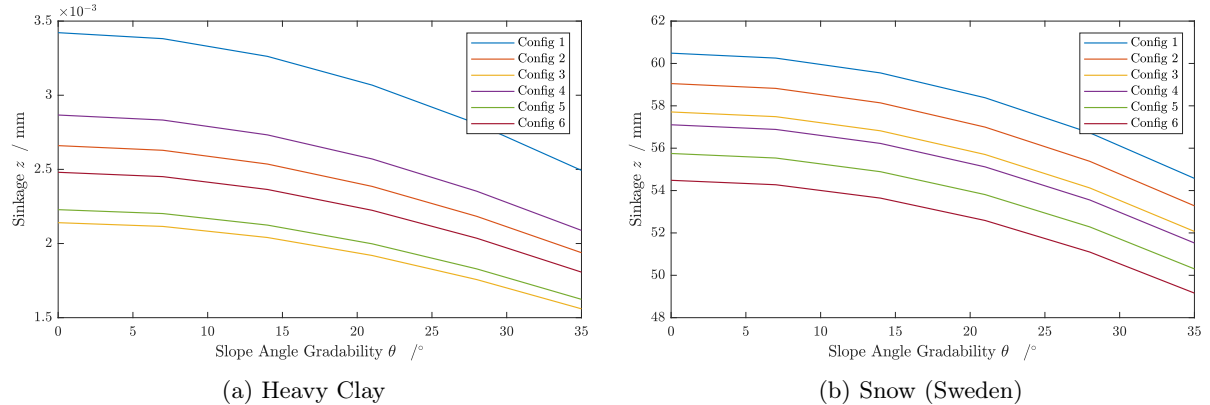


Figure 4.3: Wheel sinkage z as a function of the slope angle θ of each configuration with different soil parameters, referred to Table C.1. More information about the calculation can be found in Table H.1.

The required power for the rover can be calculated by the resistances that have to be exceeded. For the total resistance, the following applies [19]:

$$R_{\text{total}} = \underbrace{R_{\text{compaction}}}_{R_c = \frac{z^{n+1}}{n+1} (k_c + b k_\phi)} + \underbrace{R_{\text{rolling}}}_{R_r = W_w C_{rr}} + \underbrace{R_{\text{gravity}}}_{R_g = W_w \sin \theta} + \underbrace{R_{\text{bulldozing}}}_{R_b \rightarrow 0}. \quad (4.2)$$

Due to the hard surface of Europa, it can be assumed that $R_b \rightarrow 0$. In contrast to R_g , R_r can be defined as constant. With a rolling resistance coefficient of $C_{rr} = 0.02$, the resulting resistance is $R_r = 0.1972$ N [20]. Analogous to z , the lower limit of R_{total} with soil properties of heavy clay is plotted in Figure 4.4c, while the upper limit is shown in Figure 4.4d for snow.

In addition to the resistance that needs to be exceeded in order to move, a maximum limit can also be determined. The ground thrust H indicates the amount of traction that can be achieved before the wheels slip [19]. Therefore, following applies:

$$H = A \cdot c + W_w \cdot \tan \Phi, \quad (4.3)$$

4.2. LOCOMOTION

with the wheel ground contact area $A = \frac{\pi}{4} \cdot b_w \cdot l_w$ and the ground contact length $l_w = \frac{d_w}{2} \cos^{-1} \left(1 - \left(\frac{2z}{d_w} \right) \right)$. As a result, the upper limit of traction is presented in Figure 4.4a for heavy clay and Figure 4.4b for snow.

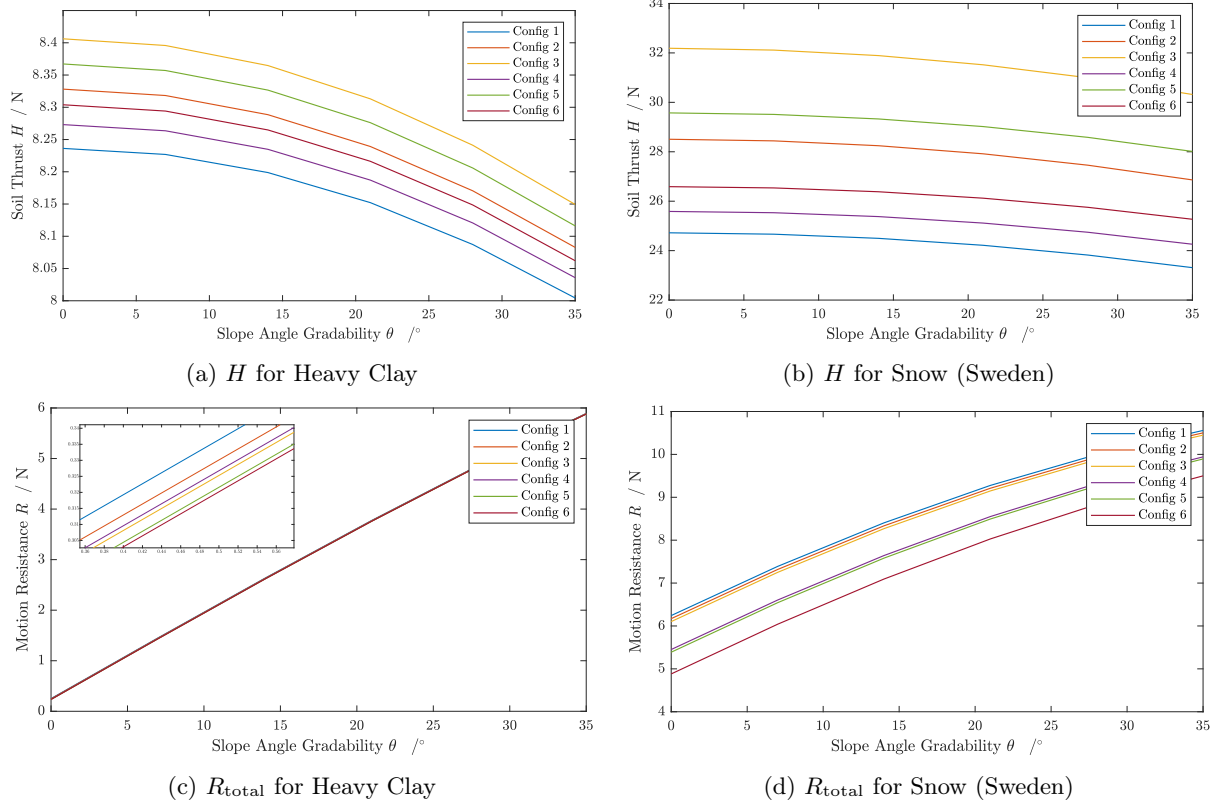


Figure 4.4: Comparison of the rover's soil thrust versus the motion resistance to exceed, each for the soil parameters of snow in Sweden and heavy clay, referenced to Table C.1. Additional information about the calculation can be found in Table H.1.

In addition to the determined parameters, it should also be verified that the mean maximum pressure (MMP) does not increase excessively due to the selected geometric parameters [21]. For this conservative calculation, a rigid wheel is assumed, whereby for the deflection δ applies, that $0 \leq \delta \leq 0.1d$ [19]. For terrestrial snow, 40 kPa should not be exceeded, but ideally the MMP should be less than 10 kPa [22]. The associated verification calculation can be found in Appendix C.1.

For the rover design, "Configuration 6" is chosen as it offers the lowest resistance to exceed whilst maintaining the lowest MMP . The $MMP_{Config6}$ is less than 40 kPa for $\delta \geq 5 \cdot 10^{-4}$, so the deflection of the wheels for the rover can be obtained to $5 \cdot 10^{-4} \leq \delta \leq 0.01$ m. Additional information of the $MMP_{Config6}$ can be found in Table H.1. It should be noted, that the rover has additional grousers. These are enhancing the traction, whereby the maximum reachable soil thrust H can be increased. However, the grousers are not taken into account in this study, as this is a conservative estimation, and the grousers can be seen as a further design improvement.

Steering

Since the rover has an all-wheel actuation, it can be operated with on-point steering and, in order to avoid greater obstacles, with Ackerman steering. Considering that with Ackerman steering the radius of the outer wheels is at a greater distance in the circumventing circle than that of

the inner wheels, the angles of the wheel positions, which are important for the control of the rover, are further examined in Appendix C.1.

Hardware Selection

For the wheel driving system, BLDC motors were chosen. In contrast to stepper motors, these are optimised for a uniform torque and not for precise motion control. The resulting power of each wheel can be calculated with respect to the required torque τ and the estimated velocity v :

$$P = \underbrace{\tau}_{R_{\text{total}}\left(\frac{d_w}{2} - \delta\right)} \left(\frac{2v}{d_w} \right). \quad (4.4)$$

The motors are designed to produce the minimum achievable power for any soil condition and a slope angle of $\theta_{\max.} = 35^\circ$, listed in Table C.3 and velocities of $0.1 \leq v \leq 1 \text{ m/s}$ are achievable. However, as indicated in Figure 4.4, higher power up to H can also be generated. Additional planetary gears increase the produced torque with a reduction ratio of 21:1 to $\tau_{\max} = 0.5 \text{ Nm}$. For the steering system, space grade stepper motors are selected, as a precise motion control is required. Additional information of the motors and gears can be found in Table H.1.

4.2.3 Deployment mechanism

The deployment mechanism enables the rover to be stored in the lander in a space-saving arrangement. Two stepper motors are activated in the axle joints for this purpose. In addition, two further inactive motors are installed for redundancy. Stepper motors have the additional advantage that they maximise the holding torque. If in a further design step it should become apparent that the torque is not sufficient, a worm gear could be installed which has a self-retaining function. In addition to deploying after landing, the mechanism is used to reduce the distance to the ground for drilling.

4.3 Electrical Power System

The EPS (Electrical Power System) is the subsystem responsible for the electrical power supply of INSPIRE. It consists of four fundamental parts, which are the energy source, the PCDU unit (Power Control and Distribution) and the Energy Storage as well as the rover subsystems as the consumers. The EPS is visualised in Figure 4.5.

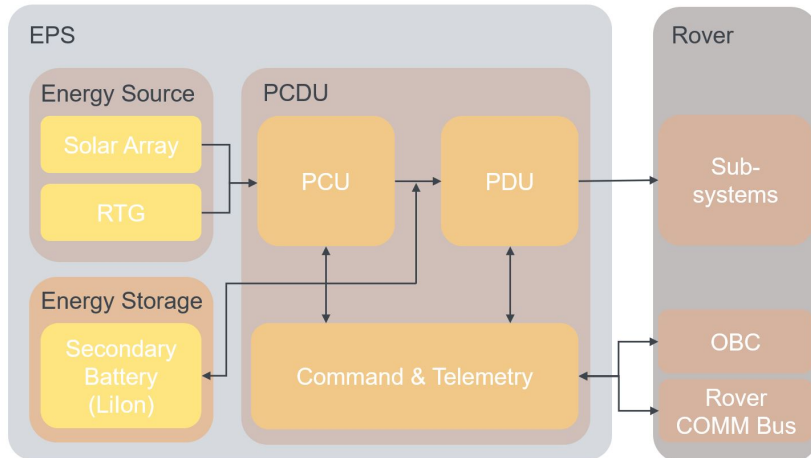


Figure 4.5: Functional Flow Chart Diagram for the EPS Subsystem.

4.3.1 EPS Budget and Overview

Figure 4.6 summarises the power budget of INSPIRE based on the rover system modes defined in Section 3.2. The holistic power budget can be found in Figure D.1.

As can be seen, the Locomotion mode has the highest demands on the EPS. The two payload modes also have a high power demand. The Communication mode also has a high consumption. However, since this is primarily used at night and the rover can be charged again afterwards without any problems, it does not place any major restrictions on the power budget. Idle/Perception mode has a low consumption, but is usually used for a long time at a stretch and therefore also places high demands on the EPS. In Charging mode, the EPS is able to charge $8.82 \text{ W}_{\text{el}}$.

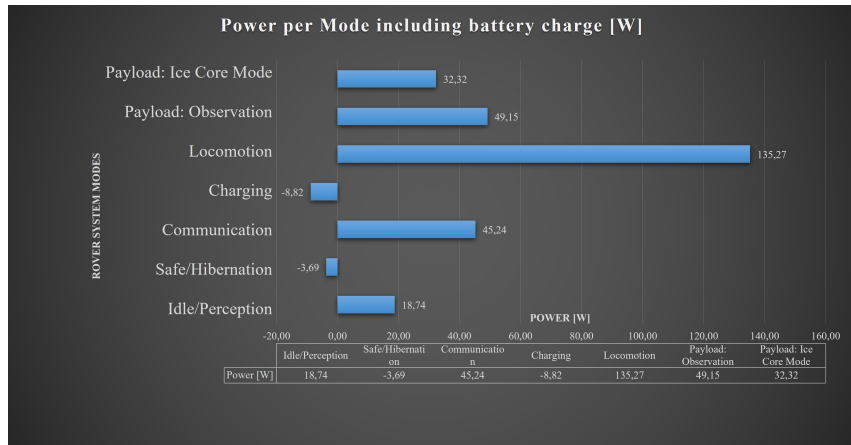


Figure 4.6: Functional Flow Chart Diagram for the EPS Subsystem.

4.3.2 Energy Source

For the energy generation of INSPIRE many possible sources were taken into consideration for a trade-off. As a conclusion of this trade-off the decision was made to utilise a Radioisotope Thermoelectric Generator (RTG) as the main energy source for INSPIRE.

As the research couldn't find an RTG with a mass suitable for INSPIRE, the solution was to scale down a bigger RTG as an approximation. As a baseline of the scaling the eMMRTG (Enhanced Multi Mission Radioisotope Thermoelectric Generator) was utilised, which is currently under development at NASA and is especially designed for deep space missions like Europa. For the scaling a goal RTG mass of $m_{\text{RTG}} = 3 \text{ kg}$ was defined and the eMMRTG was scaled down using the given data.

In Table 4.3 the scaling results for the eSMMRTG (Enhanced and Scaled Multi Mission Radioisotope Thermoelectric Generator) are listed. The eSMMRTG has a BOL specific power of $\alpha_{\text{BOL}} = 4.0 \frac{\text{W}_{\text{el}}}{\text{kg}}$ and provides an electrical power of $P_{\text{el}} = 12.08 \text{ W}_{\text{el}}$ during the mission duration [23–27].

Table 4.3: Parameters for the scaled eSMMRTG based on the eMMRTG.

Scaled eSMMRTG Parameter	Unit	Value
System Mass m_{RTG}	kg	3.5
BOL Specific Power α_{BOL}	$\frac{W_{\text{el}}}{\text{kg}}$	4.0
BOL Power $P_{\text{el,BOL}}$	W_{el}	14
Isotrop	-	Pu-238
Isotrop Half-Life	a	87.7
Flight time and Storage (incl. Margins)	a	7
Power Loss Degradation until BOM	W_{el}	0.56
BOM Power $P_{\text{el,BOM}}$	W_{el}	13.44
Europa Day Duration	h	85
Mission Duration	d	106.25
End of Mission Power $P_{\text{el,EOM}}$	W_{el}	13.42
Final Power for Study P_{el} (incl. 10 % scaling Margin)	W_{el}	12.08

Furthermore INSPIRE will also be equipped with some radiation hardend solar arrays as already explained in Section 2.5 [14]. Since these solar cells are primarily used for technology testing, the mission must also be able to operate completely without this generated energy. For this reason, and because the expected energy generated by the solar cells is minimal, only the energy generated by the RTG is considered for the Phase 0/A Study. However, it should be noted that these solar cells will also generate a certain amount of energy, which will be beneficial for the EPS.

4.3.3 Energy Storage

For the energy storage of INSPIRE many possible battery types were taken into consideration for a trade-off. As a conclusion of this trad-off the decision was made to utilise LiIon batteries as the secondary batteries of INSPIRE. This decision is primarily based on LiIon batteries high energy density, temperature range, robust performance and long operating and cycle life in extreme environments[28]

As the RTG only generates a small constant power the main energy source during the mission will be the accumulated energy of the batteries. The rover will charge the batteries at night, so the next exploration day can start with full capacity. Furthermore the batteries have to be charged during day time to maintain operations.

For the sizing of the batteries, the rover motion was chosen as the design driver, since this is the highest energy consuming state of the rover and additionally mission critical for INSPIRE. The rover motion consists of an interaction of the Locomotion and Perception mode as already mentioned in Chapter 3. Therefore it was defined that INSPIRE shall be able to drive 50 m (including alternating Locomotion and Perception Mode) with a fully charged Battery. Furthermore the battery mass shall not exceed 2 kg. The required battery capacity $C_{\text{Batt,req}}$ can be calculated using Equation 4.5. The results are listed in Table 4.4 [29].

$$C_{\text{Batt,req}} = \frac{P_{\text{el,req}} \cdot t_e}{DoD \cdot \eta_{\text{LiIon}}} \quad (4.5)$$

Using these values a suitable battery cell and battery design configuration were conducted. Under consideration of these parameters the battery capacity C_{Batt} can be calculated:

$$C_{\text{Batt}} = C_{\text{cell}} \cdot V_{\text{cell}} \cdot N \cdot M. \quad (4.6)$$

Table 4.4: Power consumption mode used as design case for the battery sizing.

Power Consumption Mode:	Unit	Locomotion	Perception
Required Electrical Power $P_{\text{el},\text{req}}$	W _{el}	135.27	18.74
Duration of the mode t_e	s	500	15000
DOD for Dimensioning	-	0.90	0.90
Efficiency of LiIon Cells η_{LiIon}	-	0.95	0.95
Required Battery Capacity per mode C_{mode}	Wh	21.97	91.33
Total Required Battery Capacity $C_{\text{Batt},\text{req}}$	Wh		113.30

According to the ECSS reliability restrictions 1 battery string must be subtracted for dimensioning. Furthermore a 30 % margin on the energy content was applied. This leads to a final battery configuration with a capacity of $C_{\text{Batt}} = 156.24$ Wh and a mass of $m_{\text{Batt}} = 1980$ g. The final battery values are listed in Table D.1 [30].

4.3.4 EPS Power Control and Distribution

In order to ensure the full functionality of the EPS, the last main component to be selected is a suitable PCDU. As described in Figure 4.5, the PCDU forms the heart of the EPS and is an important interface to the OBC and COMM. Furthermore the PCDU shall be able to monitor and control the rover system if necessary through watchdogs, HPC (High Priority Commands) and direct connections to the OBC and COMM.

The PCDU has the challenging task not only to process the RTG as the main energy source, but also to process solar cells as secondary energy sources. Therefore, a PCDU was sought which has the required size, dimensions and range of functions. The research resulted in the Nova PCDU from Bradford DSI. In addition, margins were added to the PCDU to ensure feasibility[31].

4.4 Communications and Command & Data-Handling

The Communications subsystem consists of redundant transmitters and receivers which are cross strapped to four antennas and the OBC. Additionally hard wired connections linking the communication system to the PCDU enable for reboots via direct commands (see Subsection 4.3.4). C&DH is responsible for the generation of telemetry from the housekeeping boards and the execution of tele commands, as well as the storing and compressing of payload data.

4.4.1 Operational Concept

Due to power and time constraints, the rover will transmit only telemetry during the locomotion and payload campaigns. Payload data will be compressed, stored and forwarded to the Lander at the end of a mission day.

To achieve the scientific output from Section 3.1 the transmission time per Europa day is calculated in Subsection E.2 (Table E.5) and adds up to 38.23 minutes.

4.4.2 Communication System

Requiring too many resources a direct link to earth has been deemed impractical. Instead communication for the INSPIRE mission is proposed to rely on a link between the rover and the

Europa Lander. The lander then forwards data to earth via a satellite relay carrier which orbits the moon. The lander offers a 25 dB high gain antenna [32] and a low gain antenna which is not further specified in literature.

The downlink from the rover to the lander has been identified as the critical transmission path. However, link budget considerations in Subsection E.1 reveal that a transmission to the LGA of the Europa Lander produces a link margin of 10.59 dB, resulting in a Bit Error Rate of less than 10^{-4} (reference Figure E.1). The link budget in Table E.2 has been performed under the conservative considerations listed in Table E.1.

Using the Landers LGA greatly increases robustness due to the elimination of pointing errors and higher margin for rover positioning error. Additionally, the INSPIRE rover's communication link would not interfere with the Landers communication to the relay carrier by blocking the HGA.

Component Selection

Due to the considerably high link margin the focus is on low mass and low power components with flight heritage such as flown on CubeSat missions. Criteria with relatively small impact on the link budget such as component noise or even FEC have not been taken into account. The rover communication uses X-Band for increased compatibility with the lander and has a total system mass of less than 1 kg.

Since radiation hardness was not included in most data sheets a total dose of < 20 krad was assumed in accordance with values for COTS components for LEO [33].

The selected components are listed in Table 4.5.

Table 4.5: Key criteria of selected communication components (data-sheets Table H.1).

Component	Supplier	Part Description	1. Criteria	Value	2. Criteria	Value
Transmitter	Sputnix	SXC-XTX-01	mass	0.195 kg	data rate	10 Mbit/s
Receiver	Endurosat	S-Band receiver	power	max. 2 W	mass	0.220 kg
Antenna	Endurosat	patch antenna	mass	2.2 g	frequency	X-Band

Expected transmission times per mission day are less than 40 minutes (see Subsection E.2, Table E.5). Therefore the transmitter mass is identified as more critical than power.

On the other hand receiver duty cycles are 100 % as can be found in Figure D.1. Thus power has been identified as the most crucial criteria.

A passive X-Band antenna was selected due to compact dimensions and zero power consumption. The entire trade off can be found in Table H.1.

4.4.3 Command & Data Handling

With respect to restricted power supply a redundant OBC hot-cold configuration stands to reason. Additionally, the standby mode is suggested during hibernation and charging modes relying solely on the PCDU (see Subsection 4.3.4). Emphasis for the Electronics selection is placed on flight proven radiation hardness to increase mission robustness in the high radiation environment of the Jupiter system. Criteria of less importance are CPU speed and dimensions.

Instead of designing a new OBC board a trade-off was performed among existing single board computers. SBCs provide peripheral services such as bus interfaces, timer and memory in a flight proven configuration, which promises an effective mission development.

BAE Systems provides a SBC with their flight proven Power PC750 Architecture which withstands a total radiation dose of up to 1 Mrad. The robustness comes at the cost of a 182 MHz processor speed (data-sheet in Table H.1).

Additionally a custom housekeeping board will be tasked with providing engine control peripherals and sensor read out electronics.

4.5 Thermal Control System

The main object of the Thermal Control System (TCS) is to keep the electric components within their temperature limits, listed in Table F.10. As a result of Europas low surface temperature, a small solar constant and the thin atmosphere the heat loss of the rover has to be minimised [15].

4.5.1 Concepts

The main heat source of the rover is the waste heat of the RTG (see Section 4.3), which will be led by thermal straps to the temperature sensitive components. Carbon-based straps *LyNX®* with a high thermal conductivity to density ratio will be used [34]. However, the thermal conductivity is highly dependent on the material temperature, see Figure 4.7. The curve was approximated by a cubic interpolation, Figure F.3 and Equation 5.16. To consider heat loss as a result of surface contact and radiation, the thermal conductivity was reduced about 20%. The camera, exposed

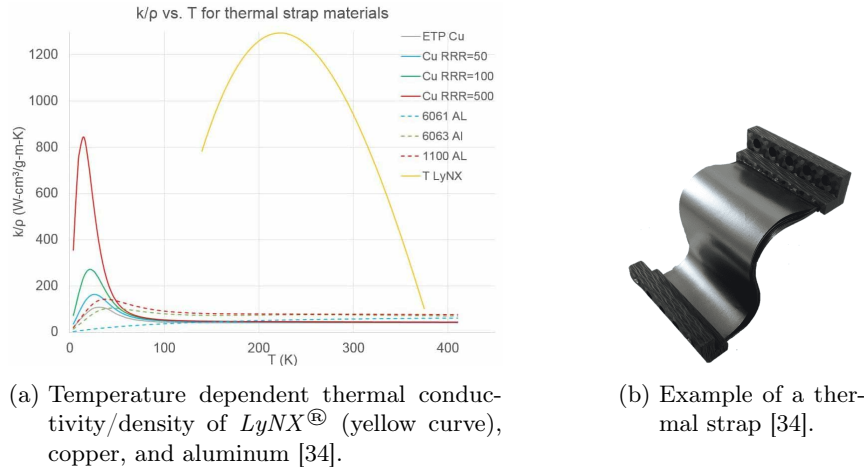


Figure 4.7: Carbon-based thermal strap *LyNX®*.

on a mast, will be heated by a separate, lightweight Radioisotope Heater Unit (RHU), which has been used during several NASA missions [35]. For the insulation, the material *Aerogel* will be applied, which has a very low heat conductivity [36].

To avoid the risk of overheating, concerning the E-bay, camera and drive engine, passive bimetallic heat switches will be placed between the application and the connection interface (see Figure 4.8). These switches change their heat conductivity beyond a certain temperature due to the expansion of the disk (see Figure 4.9a). It was assumed that the toggle temperature can be adapted by modifying the disk height. The influence of the changed disk stiffness on the contact pressure and therefore the heat conductivity was neglected for this study. The measured heat

conductivity characteristic was divided in three linear sections (Figure 4.9b), to enable a simple modelling in the thermal calculation. For most components, a cost-efficient sand blasting of the surface is applicable. For special requirements, white paint will be used, Table F.14.

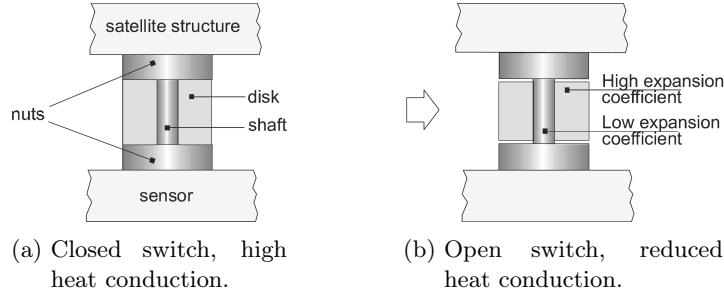


Figure 4.8: Bi-metallic heat switch [37].

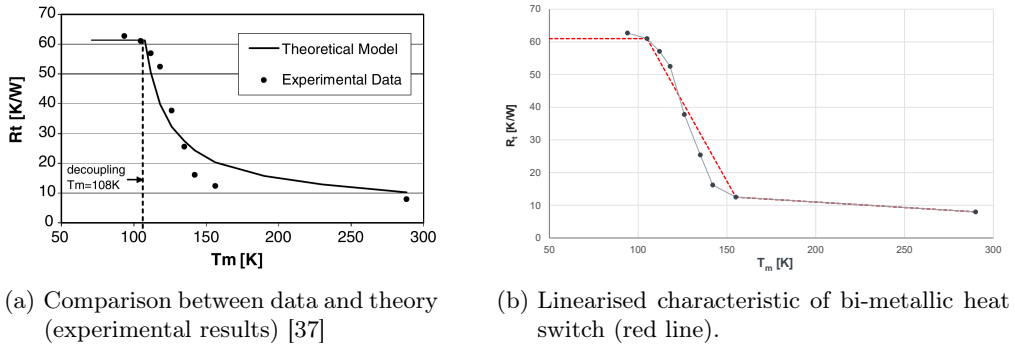


Figure 4.9: Change of the heat switch conductivity R_t over the mean temperature T_M .

4.5.2 Thermal Network

A thermal analysis was performed in order to get

- the dimension of the insulation and heat straps,
- the necessary amount of RHUs and heat switches,
- the required surface finishing and
- the suitable choice of material.

For that, a thermal network with ten nodes was derived from the rover, shown in Figure 4.10. At the intersection of the steer and drive engine, two additional nodes were defined to calculate the heat flow.

On the basis of the thermal network, the heat energy equilibrium for each node was defined (see Subsection F.2). The calculations were considered as a quasi-static analysis, where the component temperatures stay constant, $\frac{dT}{dt} = 0$. Following simplifications and assumptions for the analysis were made.

- The convection was neglected due to the thin atmosphere.
- The whole electrical power of the components will be dissipated into heat. The dissipation power of the LED ist 1.2 Watt.

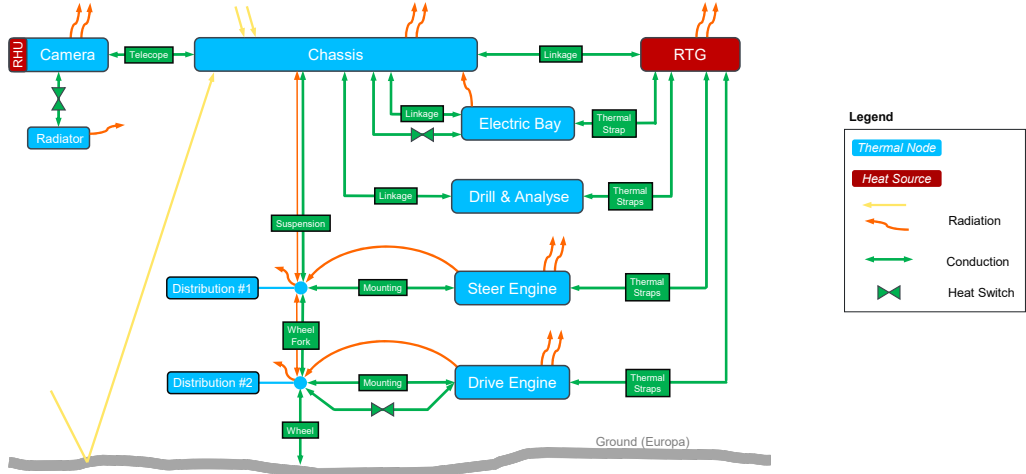


Figure 4.10: Thermal network of the rover.

- A variation of $\pm 20\%$ for the emissivity and absorptivity values was considered, if applicable (see Table F.12).
- The heat as a result of retardation radiation inside the shielding was neglected.
- No discrete nodes for the radar, hazcams, APXS and deployment engines were considered. Their heat will be led into the chassis.
- The mechanism engines weren't considered.
- For the bogies and the wheel fork radiation was defined. The radiation temperature is the mean temperature of the two connecting nodes. Half of the heat loss was added to corresponding nodes (either Chassis, Node₁ or Node₂).

4.5.3 Analysis

The thermal analysis was performed as an Excel calculation with the possibility to adapt input values and dimensions, Table H.1. The major driving load cases are the hot and the cold cases, where the maximum and minimum temperatures of the rover components will be reached. For that, the most powerful components were set to operating mode at once or only the minimum required components were turned on, respectively. The emissivity and absorptivity were adjusted to fulfil the cases. There were further load cases defined to consider the battery charging, the communication mode and the drill & analyse operation.

4.5.4 Results

The resulting temperatures for each node over all loadcases are listed in Table F.1. All temperatures lay between their limits without using a heater. The margins for uncertainties, acceptance tests and qualification tests were considered with 5 K each, ± 15 K in total [38]. The corresponding temperatures are listed in Table F.2. Due to the margin, the electric E-bay exceeds the temperature limits of the transmitter. The issue can be solved by optimising the heat paths and adding further insulation during a detailed E-bay design process. Yet another result can be found in Table F.3 to Table F.7, Table F.8 and Table F.11.

4.6 Radiation

Compared to the radiation environment near Earth the radiation environment near Jupiter is multiple times stronger. It has the highest radiation levels of any planet in our solar systems [39]. In order to survive these harsh environmental conditions, special emphasis must be placed on the radiation protection. In Figure G.1, the average trapped proton and electron fluxes on Europa's orbit around Jupiter are shown in comparison to the outer Van Allen radiation belt around Earth. However, in contrast to the Van Allen radiation belt, the duration within the radiation environment on Europa cannot be minimised and the rover has to be designed to withstand the entire mission duration of 30 days.

In order to design and evaluate different radiation protection approaches, different calculations have to be performed. For this purpose the ESA SSpace ENVironment Information System (SPENVIS) is used [40]. All calculations and figures in Section 4.6 are performed with SPENVIS unless otherwise stated.

4.6.1 Radiation Protection

Various options are available to protect the rover against the radiation. A common approach is the use of aluminium or titanium as these materials can also act as structural elements. However, due to the mass constraints of 30 kg other materials or material compositions are taken in consideration which are more mass effective. In Table 4.6, an optimised shield structure is presented for different weight thresholds designed for the radiation environment around Jupiter. The difference between an aluminium or titanium shielding and an optimised structure listed in Table 4.6 for the total ionizing dose (TID) is shown in Figure G.2.

Due to the mass savings of the optimised structure it will be used where the radiation protection of the aluminium structure is not sufficient. In order to reduce the mass further, a radiation vault is utilised that highly sensible components do not have to be shielded separately.

Table 4.6: Optimal shield structure for an Jupiter mission. [41]

Areal Density / g/cm ²	0.5	1	2	3
Layer No. 1 / mm	Pb 0.415	Pb 0.829	W 0.984	Ta 1.563
Layer No. 2 / mm	Fe 0.033	Mg 0.158	Mg 0.540	Al 0.399
Layer No. 3 / mm	-	-	-	Mg 0.150

4.6.2 Components

Every component on the rover has a different radiation tolerance and therefore have to be placed at different compartments within the rover. The radiation tolerances are listed in Table G.1. None sensitive components like the electric motors and harness are only shielded by an aluminium structure as the metal within the wire are resistant against the radiation. However, isolators around the cables have to be selected to be resistant in order to prevent short circuits. Highly sensitive components like cameras have an additional protective layer in order to reduce the TID to under 30 krad. Components which are within the rover like the on-board computer (OBC) are placed within the radiation vault which reduces the TID to under 20 krad. For this purpose the optimised shield structure with a weight target of 0.5 g/cm² is used. Detailed TIDs for all compartments are shown in Figure G.3 and for all components in Table G.1.

4.6.3 Improvements

Even though the radiation protection is sufficient for the rover to survive at least the nominal mission of 30 days, further improvements can be performed in order to extend the secondary mission or reduce the overall mass.

Local shielding can be applied on less resistant components in order to reduce the wall thickness of the whole radiation wall. If components with a radiation tolerance under 43.27 krad are individually shielded, the additional protection next to the aluminium structure can be removed. Additionally, water ice extracted from the surface of Europa can be used to improve the radiation protection. With a layer of one centimetre of water, the TID within the radiation vault can be reduced to 16.03 krad without the additional radiation protection beside the 4 mm of aluminium structure. By applying one or more of these improvement the start mass of the rover can therefore be reduced by approximately 897.2 g.

Detailed calculations for local shielding and water improvements can be found in Appendix G.3 and may be analysed further in Phase B.

4.6.4 Conclusion

In order to protect the rover against the high radiation levels at the surface of Europa, the rover has different compartments. High sensible components are placed within a radiation vault which has a mass optimised structure. Components which have to be outside the radiation vault but are highly sensible are shielded individually. Low sensible components are protected by the aluminium structure. Figure 4.11 illustrates the different compartments within the rover and the accorded TIDs.

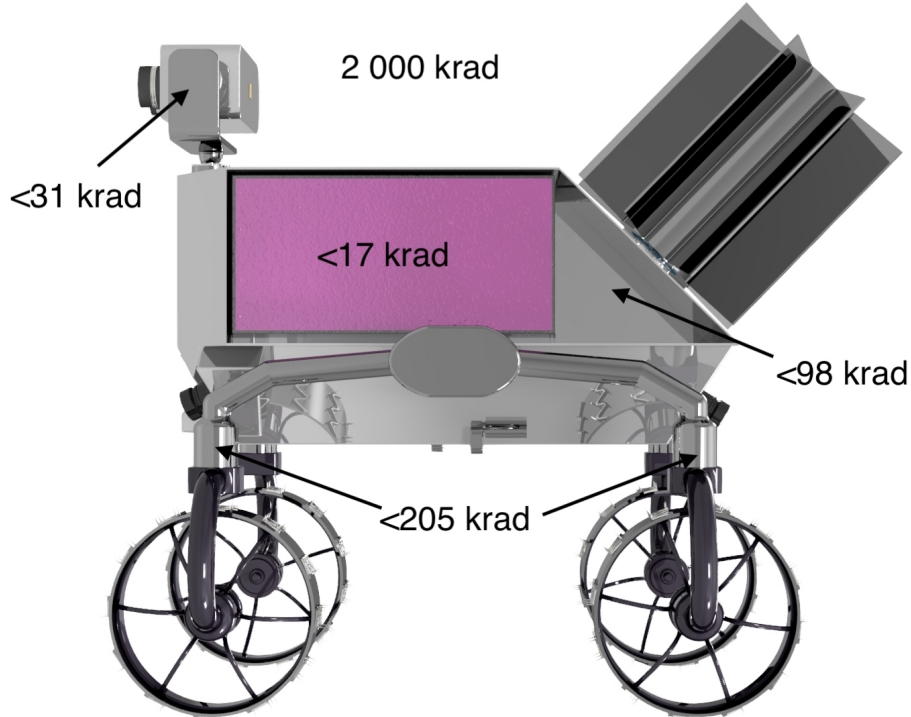


Figure 4.11: Overview of TIDs within different compartments within the rover.

Chapter 5

Outlook & Risk Assessment

5.1 Risk Assessment

To reduce risks and increase the robustness within the development process for the INSPIRE mission, all subsystems focus on flight proven or space grade hardware. Table 5.1 provides an overview on the resulting TRL for each subsystem.

Table 5.1: Subsystem TRL for risk assessment

Subsystem	overall TRL	Deviating component
Payload	0	Drill System and Sample Analyser TRL 0
Structure & Mechan.	0	Boom Mechanism TRL 0
Locomotion	0-9	Structure Components for Locomotion TRL 0
EPS	9	PCDU may be customised
TCS	4-9	none
COMs, C&DH	9	Housekeeping TRL 0

Housekeeping electronics and the boom mechanism to extend the camera head for the INSPIRE mission will be custom designed components and therefore rated at TRL 0. However due to proven development processes and simple testing the risk for the mission progress is rated non critical.

Payload components development depict the highest risk for the mission. The Analyser for the ice core samples is a downsized replica of the APXS sensor [12, 13]. The ice core drill derives from the Nano Drill offered by Honeybee Robotics [42]. Although the technology is available, the drill has to be adapted and tested. Testing in analog conditions potentially takes place in the arctic region and therefore lengthen the mission development process.

As a conclusion the payload subsystem development contains the highest risk for the INSPIRE mission. However the risk is considered manageable. Additionally investing in payload development is regarded worth the risk taking as it is integral to the successful investigation of Europa. For the TCS the dimension of the bi-metallic heat switches has to be adapted. Tests in a special environment and for qualification have to be done as well.

For the motors of the locomotion system, space grade components are selected. The stepper motors are already designed as space motors by Phytron [43]. The BLDCs of the wheel drive, on the other hand, were selected because the same series is also used in the Mars Rovers Curiosity. It should be noted, however, that these are special designs of the maxon company [44]. Therefore, no further data is available and the TRL, although already flight-proven, cannot be assumed to be 9.

5.2 Outlook

In the further design iterations, detailed simulations of the chassis and the running gear could be carried out in order to get a better understanding of where the problems of the system are and at which points mass can possibly be reduced or should be added. It could also be considered whether a less complex mechanism for unfolding the drill can be designed.

Currently, the ice core samples taken be discarded after the analysis. It could be debated whether these samples will continue to be used. The previous considerations on this topic were, on the one hand, to store the samples and bring them back to the lander in order to be able to carry out further analyses if the lander should have a gripper arm or something similar to receive the samples or, on the other hand, to melt the samples and transport them to the Electric Bay with the help of micro-pumps in order to use the water gained in this way as protection against radiation. This could serve as a replacement for the previous solution and in the best case even save mass.

For the TCS, a more detailed analysis should be carried out with the Finite-Element-Method to calculate the local heat and temperature distribution. The FE results could be used to verify and adjust the analytical analysis to get a helpful tool for fast thermal calculation to evaluate different materials or designs in the further development phases.

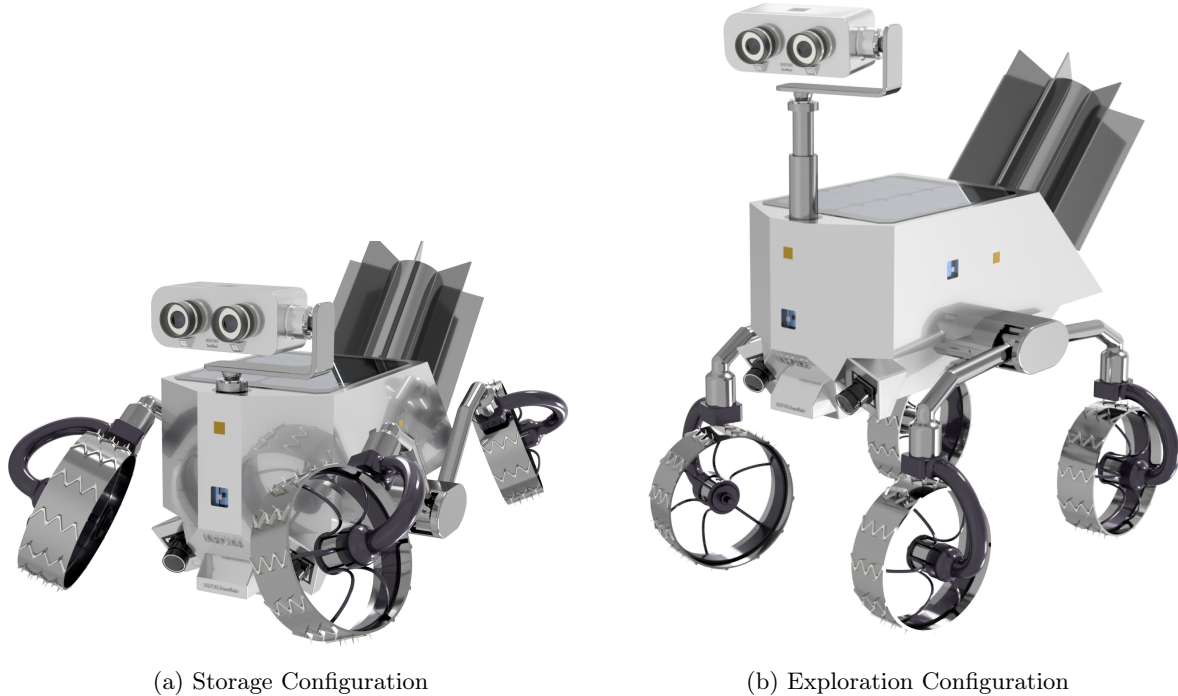


Figure 5.1: The INSPIRE rover system in it's configurations

Bibliography

- [1] Jet Propulsion Laboratory. *Galileo Mission to Jupiter*. [online] <https://www.jpl.nasa.gov/missions/galileo>.
- [2] NASA Science. *Europa Ocean Moon*. [online] <https://solarsystem.nasa.gov/moons/jupiter-moons/europa/in-depth/>.
- [3] Institut für Planetenforschung, DLR. *Die Mission JUICE zum Jupitersystem*. [online] https://www.dlr.de/pf/desktopdefault.aspx/tabid-10617/18438_read-43016/.
- [4] NASA. *Europa Lander*. [online] <https://europa.nasa.gov/>.
- [5] NASA / JPL. *Europa*. [online] <https://www.jpl.nasa.gov/missions/europa-lander>.
- [6] Soon Sam Kim Steven R. Carnes, A. F. H. C. T. U. E. H. W. N. S. A. A. “Miniature Ground Penetrating Radar, CRUX GPR”. In: *IEEEAC* (2005), pp. 1–2.
- [7] Brad A. Krainer Miig Lee, C.-C. C. and Volakis, J. D. “GPR Implications of Miniaturized Antenna Developments”. In: 2004.
- [8] Pasternack. *Microstrip Patch Antenna Calculator*. [online] <https://www.paternack.com/t-calculator-microstrip-ant.aspx>.
- [9] Honeybee Robotics. *Volatile Extractor*. [online] <https://www.honeybeerobotics.com/products/volatile-extractor/#1562267018150-cf7c081e-3ad7405c-e09c> [last accessed: 07/12/2021].
- [10] Honeybee Robotics. *Drills*. [online] <https://www.honeybeerobotics.com/products/drills/#1562267018150-cf7c081e-3ad71913-bc36> [last accessed: 07/12/2021].
- [11] DLR. *Philae Lander Fact Sheet*. [online] https://www.dlr.de/dlr/Portaldata/1/Resources/documents/Philae_Lander_FactSheets.pdf [last accessed: 07/14/2021].
- [12] Gironés, J.; Schmanke, D.; Klingelhoefer, G.; Maul, J.; Brueckner, J.; Duston, C., and Gellert, R. “The Alpha Particle X-Ray Spectrometer APXS on the Rosetta lander Philae to explore the surface of comet 67P/Churyumov-Gerasimenko”. In: (Jan. 2010), pp. 612–.
- [13] Science, N. *APXS*. [online] <https://mars.nasa.gov/msl/spacecraft/instruments/apxs/>.
- [14] Fraunhofer Institute for Solar Energy Systems ISE. *RadHard Project Website*. 2021. [online] \url{https://radhard.org/}.
- [15] “The surface temperature of Europa”. In: *Heliyon* 5.6 (2019), e01908. ISSN: 2405-8440. DOI: <https://doi.org/10.1016/j.heliyon.2019.e01908>.
- [16] Aluminium Giesserei Hannover GmbH. *Produktdatenblatt AA 7075*. [online] https://www.leichtmetall.eu/site/assets/files/datenblatt/7075_Produktdatenblatt_A4.pdf.
- [17] JPL Solar System Dynamics. *Europa By The Numbers*. [online] <https://solarsystem.nasa.gov/moons/jupiter-moons/europa/by-the-numbers/> [last accessed: 07/13/2021].
- [18] Svetlana Shekhtman, NASA. *NASA Scientists Confirm Water Vapor on Europa*. [online] <https://www.nasa.gov/feature/goddard/2019/nasa-scientists-confirm-water-vapor-on-europa> [last accessed: 07/11/2021].
- [19] Ellery, A. “Environment–robot interaction—the basis for mobility in planetary microrovers”. In: *Robotics and Autonomous Systems* 51.1 (2005). Mobile Robotics in the United Kingdom, pp. 29–39. ISSN: 0921-8890. DOI: <https://doi.org/10.1016/j.robot.2004.08.007>. [online] <https://www.sciencedirect.com/science/article/pii/S0921889004002015>.

- [20] Hoffman, A.; Steen-Larsen, H.; Christianson, K., and Hvidberg, C. “A low-cost autonomous rover for polar science”. In: *Geoscientific Instrumentation, Methods and Data Systems* 8 (June 2019), pp. 149–159. DOI: 10.5194/gi-8-149-2019.
- [21] M. Saarilahti, University of Helsinki. *SOIL INTERACTION MODEL*. [online] <https://helda.helsinki.fi/bitstream/handle/1975/8020/EC0031.pdf?sequence=3&isAllowed=y> [last accessed: 07/13/2021].
- [22] J.Y. Wong. *Theory of Ground Vehicles. Third Edition*. New York: John Wiley and Sons, 2001. ISBN: 0-471-35461-9.
- [23] R. Abelson et al. *Enabling Exploration with Small Radioisotope Power Systems*. Ed. by NASA JPL. 2004.
- [24] S. Magdum. *Model Based Development of The Enhanced Multi-Mission Radioisotope Thermoelectric Generator and Effect of Thermoelectric Element Length on eMMRTG*. Ed. by Western Michigan University. 2019. [online] \url{http://homepages.wmich.edu/~leehs/ME539/Final%20Presentation%20on%20eMMRTG.pdf}.
- [25] Holgate, T. C.; Bennett, R.; Hammel, T.; Caillat, T.; Keyser, S., and Sievers, B. “Increasing the Efficiency of the Multi-mission Radioisotope Thermoelectric Generator”. In: *Journal of Electronic Materials* 44.6 (2015), pp. 1814–1821. ISSN: 0361-5235. DOI: \url{10.1007/s11664-014-3564-9}.
- [26] JPL NASA. *Enhanced Multi-Mission Radioisotope Thermoelectric Generator (eMMRTG) Concept*. Ed. by NASA JPL. 2014. [online] \url{https://rps.nasa.gov/resources/56/enhanced-multi-mission-radioisotope-thermoelectric-generator-emmrtg-concept/}.
- [27] Lakdawalla, E. *The Design and Engineering of Curiosity*. Cham: Springer International Publishing, 2018. ISBN: 978-3-319-68144-3. DOI: \url{10.1007/978-3-319-68146-7}.
- [28] S. Fasoulas et al. *Lecture Series: Energy Systems for Space Application SS 2020*. 2020.
- [29] S. Klinkner; P. Winterhalder, and M.Nitz et al. *Lecture Series - Rover System Technology SS2021*. 2021.
- [30] SAFT Batteries. *Datasheet - SAFT MP 176065 xlr*. 2018. [online] \url{https://www.saftbatteries.com/products-solutions/products/mp-small-vl}.
- [31] BRADFORD ENGINEERING BV, ed. *Datasheet - Nova PCDU*. 2019. [online] \url{https://satsearch.co/products/bradford-nova-pcdu}.
- [32] Nacer Chahat Brant Cook, H. L. and Estabrook, P. “All-Metal Dual-Frequency RHCP High-Gain Antenna for a Potential Europa Lander”. In: () .
- [33] Dough Sinclair, J. D. “Radiation Effects and COTS Parts in SmallSats”. In: *27th Annual AIAA/USU Conference on Small Satellites*. Sinclair, 2013, p. 2.
- [34] Thermal Space and Thermal Straps. *Graphene Thermal LyNX® Technology*. [online] <https://thermal-space.com/thermal-lynx/>.
- [35] NASA. *Light-Weight Radioisotope Heater Unit*. [online] <https://rps.nasa.gov/power-and-thermal-systems/thermal-systems/light-weight-radioisotope-heater-unit/>.
- [36] NASA / JPL. *Aerogel*. [online] <https://solarsystem.nasa.gov/stardust/aerogel.pdf>.
- [37] Milanze, F. H. and Mantelli, M. B. “Theoretical and experimental studies of a bi-metallic heat switch for space applications”. In: *International Journal of Heat and Mass Transfer* 46.24 (2003), pp. 4573–4586. ISSN: 0017-9310. DOI: [https://doi.org/10.1016/S0017-9310\(03\)00294-1](https://doi.org/10.1016/S0017-9310(03)00294-1).
- [38] S. Klinkner date = 2020, t. T. i. I.

- [39] astronomy.com. *What is the source of Jupiter's radiation?* [online] <https://astronomy.com/magazine/ask-astro/2020/02/what-is-the-source-of-jupiters-radiation> [last accessed: 07/18/2021].
- [40] ESA. *SPENVIS*. [online] <https://www.spenvis.oma.be> [last accessed: 07/18/2021].
- [41] Wang, J.-Z.; Ma, J.-N.; Qiu, J.-W.; Tian, D.; Zhu, A.-W.; Zhang, Q.-X., and Zhou, A.-S. "Optimization Design of Radiation Vault in Jupiter Orbiting Mission". In: *IEEE Transactions on Nuclear Science* 66.10 (2019), pp. 2179–2187. DOI: 10.1109/TNS.2019.2939184.
- [42] Zacny, K.; Paulsen, G.; Chu, P.; Hedlund, M.; Spring, J.; Osborne, L.; Matthews, J.; Zarzhitsky, D.; Nesnas, I. A.; Szwarc, T., and Indyk, S. "Axel rover NanoDrill and Powder-Drill: Acquisition of cores, regolith and powder from steep walls". In: *2013 IEEE Aerospace Conference*. 2013, pp. 1–11. DOI: 10.1109/AERO.2013.6497188.
- [43] phySPACE. *Stepper Motor Series for SPACE applications, Standard and Customised Solutions*. [online] https://www.phytron.eu/fileadmin/user_upload/produkte/motoren_aktuatoren/pdf/ds-physpace-en.pdf [last accessed: 07/15/2021].
- [44] Maxon. *EC 32 flat*. [online] https://www.maxongroup.de/medias/sys_master/root/8839930445854/DE-282.pdf [last accessed: 07/15/2021].
- [45] Paetschke, S. *Exercise 5 - Satellite Operations using the example of the small satellite Flying Laptop*. 2020.
- [46] Susann Paetschke, J. B. *Lecture Series - Satellite Operations using the example of the small satellite Flying Laptop*. 2020.
- [47] Jun Takada Shuji Senada, H. H. M. H. T. O. S. H. M. S. S. I. "A Fast Progressive Lossless Image Compression Method for Space and Satellite Images". In: *IEEE* (Sept. 2007), pp. 479–481.
- [48] GmbH, A. G. H. *Produktdatenblatt AA5083*. [online] https://www.leichtmetall.eu/site/assets/files/datenblatt/5083_Produktdatenblatt_A4.pdf.
- [49] GmbH, A. G. H. *Produktdatenblatt AA6082*. [online] https://www.leichtmetall.eu/site/assets/files/datenblatt/6082_Produktdatenblatt_A4.pdf.
- [50] Deutsche Edelstahlwerke. *1.4418X4 - CrNiMo16-5-1*. [online] https://www.dew-stahl.com/fileadmin/files/dew-stahl.com/documents/Publikationen/Werkstoffdatenblaetter/Luft_Raumfahrt/1.4418_de.pdf.
- [51] Edelstahlwerke, D. *Firmodur 7225*. [online] https://www.dew-stahl.com/fileadmin/files/dew-stahl.com/documents/Publikationen/Werkstoffdatenblaetter/Baustahl/1.7225_1.7227_de.pdf.
- [52] thyssenkrupp Material Schweiz. *Titan 6Al4V "ELI"*. [online] https://d2zo35mdb530wx.cloudfront.net/_binary/UCPthyssenkruppBAMXSchweiz/de/downloads/werkstoffdatenblaetter-titan/link-titan_grade_5_elis.pdf.
- [53] thyssenkrupp Material Schweiz. *Titan Grade 5*. [online] https://d2zo35mdb530wx.cloudfront.net/_binary/UCPthyssenkruppBAMXSchweiz/de/downloads/werkstoffdatenblaetter-titan/link-titan_grade_5.pdf.

Appendix

A Operation

Number	Rover System Modes	Abbreviation	Definition
0	Launch/Off Mode	OFF	From Launch until EDL Phase Rover System is OFF Exact mode description t.b.d. and can be adapted to meet the lander demands Health tests on Occasion during flight time are foreseen (PCDU could be active) Batteries on Storage Capacity at launch and may be recharged on occasion (like Rosetta Mission) Telemetry data shall be sent by the Lander (optional if possible) RTG on =>Electrical and Thermal Power may be used (for Lander Power and Thermal Systems) or is disposed of by shunts
1	Entry, Descent and Landing	EDL	From Entry until next morning after secure landing of Lander on Europa See Mode OFF PCDU ON after secure landing (Powered by RTG) Heaters ON (powered by remaining RTG Power) Battery charging if no Kill Switch is used First Morning after EDL Exact mode description t.b.d. and can be customized to lander =>Dependant on final Lander Design Critical Deployments (Egress System) and leaving the lander Optional whether Kill Switch ejected =>Battery charging can start
2	Deployment and Early Operation Mode	EOP	Rover System Activation possibilities: Kill Switch, Lander Interface, HPC from Earth PCDU ON OBC ON Heaters ON After sufficient Battery Capacity is reached (50%): Deployment of Rover Boogie and checkout/health check of all Rover Systems Afterward switching to Charging Mode
3	Idle/ Perception	ID	During Idle Operation Time Rover powered by RTG or Batteries (Excess Power charges Batteries) PCDU ON All Components in Standby or Power Saving Mode if possible Stereovision Camera ON for Orientation and Observation (Science Data) Hazcams and OBC ON for Orientation and Path Analysation COMM ON for larger time intervals (Listening Mode)
4	Safe Mode/ Hibernation (SAFE)	SAFE	Entered in case of emergency or contingency Rover Survival Mode =>Minimum Power PCDU ON COMM sends Emergency Signal then switches to COMM ON for small time intervals (Listening Mode) OBC OFF until Command received =>High Power Commands (HPC) Heaters ON Science data shall be stored without data loss Applicable during Day and Nighttime Exit after receiving the corresponding command (Optional: Timer ON and Restart of Rover System after time period has passed)
6	Communication	COMM	During Transmission of major Telemetry or Science Data Rover powered by RTG or Batteries (Excess Power charges Batteries) PCDU ON All Components in Standby or Power Saving Mode if possible OBC SB COMM ON (Transmission Mode)
7	Charging	BAT	For Battery charging Rover batteries charged by RTG PCDU ON All Components in Standby or Power Saving Mode if possible OBC SB Quit after sufficient charge is reached
8	Locomotion	LOC	For Rover Movement and Observation Locomotion and Navigation ON Hazcams and Traversing Path Analysis ON OBC ON PCDU ON COMM OFF Stereovision Camera ON for Orientation and Observation (Science Data) Only during Daytime
9	Payload Observation Mode	OBS	Payload Mode for Science Data Collection during Daytime OBC ON PCDU ON COMM OFF Stereovision Camera ON for Orientation and Observation (Science Data) RADAR ON for Ground Investigation =>Drill Location Only during Daytime
10	Payload: Ice Core Mode	ICE	Payload Mode for Science Data Collection during Daytime or Nighttime OBC ON PCDU ON COMM OFF Ice Core Drill ON during Ice Core Sample Collection Afterwards Sample will be analysed =>APXS ON

Table A.1: Collection of Rover System Modes.

B Structure and Mechanism

Table B.1: INSPIRE mass budget.

Subsystem	Component Name	Mass per Component / kg	Quantity	Component Margin	Total / kg
Structure & Mechanism	Harness	3	1	20%	3.60
	Chassis	look up at Chassis Table	1	20%	5.02
	E-Bay Box	1.033	1	20%	1.24
	Boom	0.17	1	20%	0.20
	Solar Cell Plate	0.121	1	20%	0.15
Locomotion	wheels	0.158	4	20%	0.76
	rims	0.162	4	20%	0.78
	motor (wheels)	0.057	4	10%	0.25
	planetary gear(wheels)	0.118	4	10%	0.52
	Motor (steering)	0.07	4	5%	0.29
	Motor (deployment)	0.07	6	5%	0.44
	IMU	0.012	4	10%	0.05
EPS	Battery	1.98	1	10%	2.18
	RTG	3.5	1	10%	3.85
	SolarCells	0.0012975	10	20%	0.02
	PCDU	0.33	1	20%	0.40
Communication	LGAs	0.002	4	5%	0.01
	Transmitter	0.195	2	5%	0.41
	Receiver	0.22	2	10%	0.48
	Multiplexer	0.065	2	5%	0.14
C&DH / sensors	Sun Sensors	0.016	4	5%	0.07
	OBC	0.35	2	5%	0.74
	temperature Sensor	0.0002	20	20%	0.00
	Housekeeping	0.2	1	5%	0.21
Thermal Control System	Heaters	0.00181	10	5%	0.002
	isolation	0.07	1	20%	0.08
	Carbon Straps	0.48	1	5%	0.5
	RHU	0.3	1	5%	0.32
	Bi-metallic Heat Switch	0.06	10	10%	0.66
Payload	Ice Core Drill Motor & Electronics	1.3	1	20%	1.56
	Ice Core Drill Titanium bit	0.041	1	20%	0.05
	Groundradar electronics	0.045	1	5%	0.05
	Ground Radar antenna	0.00273	2	10%	0.01
	APXS Analyzer	0.43	1	20%	0.52
	Haz Cams	0.064	3	5%	0.20
	Stereo Vision Cam	0.064	2	5%	0.13
	objective StereoCam	0.08	2	20%	0.19
	objective HazCam	0.048	3	20%	0.17
	LEDs	0.003	16	10%	0.05
Radiation	Cam shielding	0.02905	5	20%	0.17
	E-Bay shielding	0.94	1	20%	1.13
Mass incl. Component Margins					27.25
System Margin					10%
Total Mass of INSPIRE					29.97

Table B.2: INSPIRE chassis mass budget.

Component Name	Mass per Component / kg	Quantity	Component Margin	Total / kg
Cam Head Box	0.223	1	20%	0.27
CamHead Fork	0.119	1	20%	0.14
Frontplate	0.165	1	20%	0.20
Sideplate	0.244	2	20%	0.59
Backplate	0.16	1	20%	0.19
Topplate	0.32	1	20%	0.38
Drillingbay	0.433	1	20%	0.52
Midplate	0.491	1	20%	0.59
Differential	0.237	1	20%	0.28
Faulhaber Motor	0.015	4	20%	0.07
IceCoreDeployment Housing	0.005	4	20%	0.02
Trapdoor	0.047	2	20%	0.11
DrillFork1	0.011	1	20%	0.01
DrillFork2	0.017	1	20%	0.02
Wheel Fork	0.122	4	20%	0.59
Gear & Motor Housing (Driving)	0.015	4	20%	0.07
Deployment Mechanism Housing	0.118	2	20%	0.28
Bogie	0.11	4	20%	0.53
HazCamBox_Front	0.046	2	20%	0.11
HazCamBox_Heck	0.027	1	20%	0.03
GroundRadarAntenna holder	0.03	1	20%	0.04
Mass with Component Margins				5.02
System Margin				10%
Total Mass				5.52

C Locomotion

C.1 Locomotion Design Drivers

In this section all necessary values for the design of the locomotion system are presented. In Section C.1 shows the geometric parameters of the locomotion system in a top view of the rover.

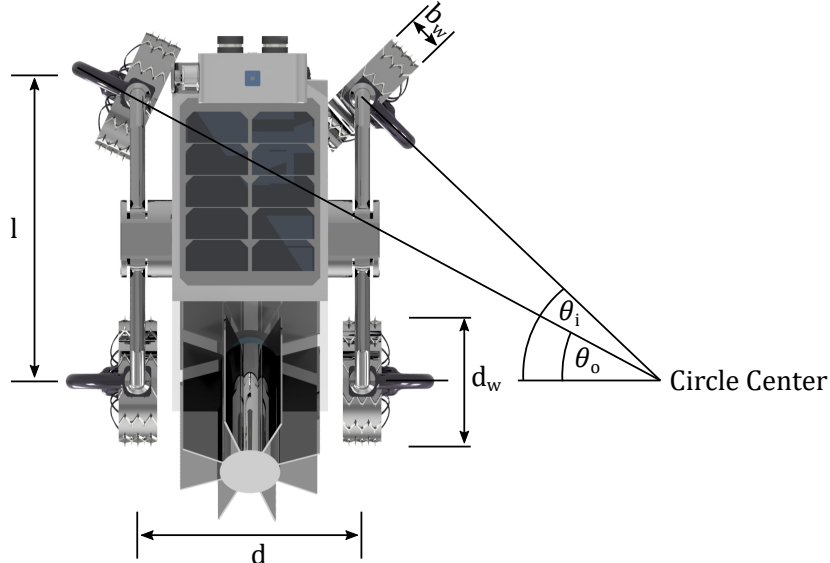


Figure C.1: Geometric dimensions for the locomotion system.

The parameters for the soils are taken from the literature [22]. Here, a hard soil was chosen as the lower boundary and a substitute for ice, heavy clay, and snow from Sweden for the upper boundary. All calculations were performed and plotted using MATLAB®. Further information on the files can be found in Table H.1.

Table C.1: Soil parameters for both soils considered: heav clay as hard equivalent for ice values and snow in Sweden [22].

Terrain	$n / \frac{\text{kN}}{\text{m}^{n+1}}$	k_c	$k_\phi / \frac{\text{kN}}{\text{m}^{n+2}}$	c / kPa	ϕ / deg
Heavy Clay	0.13	12.70	1555.95	68.95	34
Snow (Sweden)	1.44	10.55	66.08	6	20.7

Ackerman Steering

As mentioned in Section 4.2.2, with Ackerman steering it is important to take into account that the angles of the front wheel positions differ:

$$\cot \theta_i - \cot \theta_o = -\frac{d}{l}. \quad (5.1)$$

With a wheel distance of $d = 277$ mm and $l = 365$ mm, the respective angles of the wheel positions can be determined. These values are necessary to control the drive in an autonomous drive mode.

C. LOCOMOTION

Table C.2: Various wheel dimensions respective to the weight. Highlighted fields in red are not considered further for system design due to the limit of 200 g weight per wheel.

Wheel Width m	Wheel Diameter m	Weight per Wheel g	Wheel Width m	Wheel Diameter m	Weight per Wheel g
0.05	0.1	127	0.05	0.15	185
0.06	0.1	153	0.06	0.15	221
0.07	0.1	178	0.07	0.15	258
0.08	0.1	204	0.08	0.15	294
0.09	0.1	229	0.09	0.15	331
0.1	0.1	265	0.1	0.15	367
0.05	0.125	154	0.05	0.2	236
0.06	0.125	185	0.06	0.2	284
0.07	0.125	217	0.07	0.2	332
0.08	0.125	247	0.08	0.2	379
0.09	0.125	278	0.09	0.2	427
0.1	0.125	309	0.1	0.2	487

Mean Maximum Pressure

To determine the mean maximum pressure, the data are taken from Figure C.2.

Number of axles	Proportion of axles driven						
	1	3/4	2/3	3/5	½	1/3	1/4
2	3.65				4.40		
3	3.90		4.35			5.25	
4	4.10	4.44			4.95		6.05
5	4.32			4.97			
6	4.6		5.15		5.55	6.20	

Figure C.2: Parameters for the mean maximum pressure for a wheeled rover.

The rover has 4 number ox axles, each with a quarter proportion of axles driven. Thus, the *MMP* can be calculated to:

$$MMP = \frac{K \cdot W}{2Nb_w^{0.85} d_w^{1.15} (\delta/d_w)^{0.5}}, \quad (5.2)$$

with $K = 6.05$ and the number of wheels $N = 4$. The resulting *MMP* for the 6 considered configurations are shown in Figure C.3.

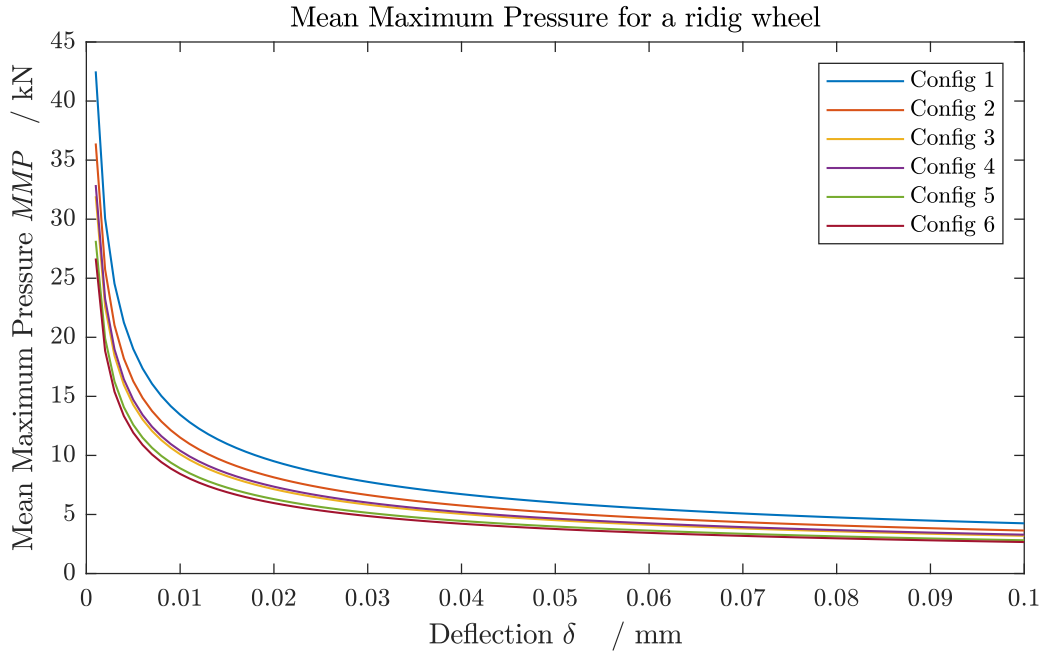


Figure C.3: Mean maximum pressure plotted over the deflection δ . The maximum value of 40 kPa is only exceeded for very small values of δ .

Hardware Selection

Each wheel has a separate BLDC motor for driving. The necessary torque is listed for both soil parameters depending on the slope angle. In addition, necessary power is listed for different velocities to be reached, also for both soils. It should be noted, that the deflection δ is not considered for this conservative estimation, though it is in the range of $5 \cdot 10^{-4} \leq \delta \leq 0.01$ m for the chosen configuration 6 .

Table C.3: Calculated torque and power of the configuration 6 in respect to the slope angle and velocity.

θ deg	$R_{\text{total,Snow}}$ N	τ_{snow} Nm	$R_{\text{total,HeavyClay}}$ N	$\tau_{\text{HeavyClay}}$ Nm	v $\frac{m}{s}$	$P_{\text{Min.,Snow}}$ W	$P_{\text{Min.,HeavyClay}}$ W
0	4.882	0.244	0.234	0.012	0.2	0.976	0.047
7	6.040	0.302	1.436	0.072	0.35	2.114	0.503
14	7.094	0.355	2.618	0.131	0.5	3.547	1.309
21	8.028	0.401	3.765	0.188	0.65	5.219	2.447
28	8.833	0.442	4.857	0.243	0.8	7.067	3.886
35	9.499	0.475	5.880	0.294	0.95	9.024	5.586

D Electrical Power System

Table D.1: INSPIRE battery parameters.

SAFT 176065 xlr [30]	
Configuration:	
Battery Configuration	<i>3s4p</i>
Cells in Series s N [-]	3
Cells in Parallel p M [-]	4
Cell Parameters:	
Typical Cell Capacity [Ah]	6.8
Nominal Cell Voltage [V]	3.65
Nominal Cell Capacity [Wh]	24.8
Typical Cell Mass [kg]	0.15
Energy Density [Wh/kg]	165.33
Actual Battery Configuration Parameters:	
Battery Voltage V_{Batt} [V]	10.95
Battery Nominal Capacity E_{Batt} [Wh]	297.6
Battery Mass [kg]	1.8
Battery Mass m_{Batt} (incl. 10% Margin) [kg]	1.98
Configruation according to ECSS reliability restrictions and margins included:	
Battery Configuration	<i>3s3p</i>
Cells in Series s N [-]	3
Cells in Parallel p M [-]	3
Battery Voltage V_{Batt} [V]	10.95
Battery Nominal Capacity E_{Batt} [Wh]	231.60
30% Margin on Energy Content	0.3
Battery Nominal Capacity E_{Batt} incl. Margin [Wh]	156.24
Useable Energy Density [Wh/kg]	78.91

Subsystem	Unit	Power demand per Unit w/o margins [W]			EDL			Deployment Mode			Idle Perception			Safe Hibernation			Communication			Charging (RTG)			Locomotion			Payload Observation				
		Amount [-]	Maturity Level	Margin (%)	Standby Status (SB) (ON)	ON Status (ON)	Nominal Max (MAX)	Duty Cycle [W]	Power Status	Duty Cycle [W]	Power Status	Duty Cycle [W]	Power Status	Duty Cycle [W]	Power Status	Duty Cycle [W]	Power Status	Duty Cycle [W]	Power Status	Duty Cycle [W]	Power Status	Duty Cycle [W]	Power Status	Duty Cycle [W]	Power Status	Duty Cycle [W]	Power Status	Duty Cycle [W]		
Payload	Ice Core Drill	1	20.00%	0	1	1.2	OFF	0	OFF	0	OFF	0	OFF	0	OFF	0	OFF	0	OFF	0	OFF	0	OFF	0	MAX	50%	7.2			
	APXS Analyzer	1	20.00%	0	0.1	1	OFF	0	OFF	0	OFF	0	OFF	0	OFF	0	OFF	0	OFF	0	OFF	0	OFF	0	MAX	50%	0.6			
	Stereo Vision Camera	2	5.00%	0	2	4	OFF	0.50%	ON	2.1	ON	20%	0.64	ON	0	OFF	0	ON	100%	4.2	ON	100%	4.2	OFF	0	MAX	25%	0.275		
	Ground RADAR	4	5.00%	0	2	4	OFF	0.50%	ON	4.2	ON	20%	1.68	ON	0	OFF	0	ON	100%	8.4	ON	100%	8.4	OFF	0	MAX	25%	0		
	LID Lumes	16	20.00%	0	0.1	1	OFF	0	OFF	0	OFF	0	OFF	0	OFF	0	OFF	0	OFF	0	OFF	0	OFF	0	ON	100%	14.4			
Command & DH	OBIC	1	5.00%	1	8	10	OFF	0	ON	10%	0.4	MAX	9.45	SH	100%	1.05	ON	100%	8.4	ON	100%	8.4	ON	100%	8.4	ON	100%	8.4		
	Housekeeping	1	20.00%	0	1	2	OFF	0	ON	10%	0.12	ON	10%	0.12	ON	100%	0.12	ON	100%	1.2	ON	100%	1.2	ON	100%	1.2	ON	100%	1.2	
Thermal Control System	Heaters	2	5.00%	0	1	2	ON	100%	2.1	ON	50%	0	0	0	0	0	0	0	0	0	0	0	0	0	0	0	0	0	0	
Electric Power Supply	PDU	1	20.00%	0.6	1	SB	100%	0.72	SB	100%	0.72	ON	100%	1.2	SH	100%	0.72	ON	100%	1.2	ON	100%	1.2	ON	100%	1.2	ON	100%	1.2	
Communication	Transmitter	1	5.00%	0.6	10	15	OFF	0	OFF	0	OFF	0	OFF	0	OFF	0	MAX	100%	0.75	OFF	0	OFF	0	OFF	0	OFF	0	OFF	0	
	Receiver	1	20.00%	0.15	1	2	OFF	0	ON	100%	1.2	ON	100%	1.2	ON	100%	1.2	ON	100%	1.2	MAX	100%	2.4	SB	100%	0.42	ON	100%	1.2	
Locomotion	Motor (wheel(s))	4	20.00%	0	9	15	OFF	0	OFF	0	OFF	0	OFF	0	OFF	0	OFF	0	OFF	0	OFF	0	OFF	0	ON	100%	2.1	ON	100%	2.1
	Motor (steering)	4	5.00%	0	2	4	OFF	0	OFF	0	OFF	0	OFF	0	OFF	0	OFF	0	OFF	0	OFF	0	OFF	0	ON	100%	1.2	ON	100%	1.2
	IMU (Deployment)	2	5.00%	0	1	2	OFF	0	ON	100%	4.4	ON	5%	0.22	OFF	0	ON	100%	4.4	OFF	0	ON	100%	4.4	ON	100%	4.4	ON	100%	4.4
Class & Structure	Boom Mechanism	1	20.00%	0	8	OFF	0	ON	100%	9.6	OFF	0	OFF	0	OFF	0	OFF	0	OFF	0	OFF	0	OFF	0	OFF	0	OFF	0	OFF	0
	Drill Mechanism	1	20.00%	0	3	3	OFF	0	OFF	0	OFF	0	OFF	0	OFF	0	OFF	0	OFF	0	OFF	0	OFF	0	OFF	0	OFF	0	OFF	0
	Cam Reluctor Motors	2	5.00%	0	2	4	OFF	0	ON	100%	2.1	ON	20%	0.42	OFF	0	OFF	0	OFF	0	OFF	0	OFF	0	ON	100%	2.1	ON	100%	2.1
S/C Net Power Demand [W]																														
Power Distribution Losses																														
Load Distribution (PDU)																														
PDU Margin (Computers, etc.)																														
Inmarsat Services																														
Additional Services ...																														
S/C Brutto Power Demand [W]																														
System Margin [W]																														
Required power from Battery (20% System Margin) [W]																														
Total Rover Power Demand excluding battery charge																														
Charging Power (5% - Union Efficiency) [W]																														
Incoming Power RTG																														
Total Rover Power Demand including battery charge [W]																														
Total Rover Power Demand [W]																														

Figure D.1: Holistic Power Budget of INPSIRE.

E Communications

E.1 Link Budget

Link budget considerations are performed under the conservative assumptions listed in Table E.1.

Table E.1: Transmission link parameters.

Parameter	Value	Unit	Symbol	Source
<hr/>				
Rover				
antenna Gain	2	[dB]	G_R	omnidirectional LGA
output power	1	[W]	P_R	Digital Appendix
line loss	0.6	[dB]	L_{l1}	[45]
<hr/>				
Path				
R2L polarisation loss	0.3	[dB]	L_p	[45]
free space loss	117.55	[m^3]	L_s	Equation 5.3
atmospheric loss	0	[dB]	L_a	negligible atmosphere
<hr/>				
Lander				
antenna Gain	1	[dB]	G_L	conservative estimation
output power	5	[W]	P_L	conservative estimation
pointing Loss	0	[dB]	n/a	omnidirectional LGA
line Loss	0.6	[dB]	L_{l2}	[45]
eff. noise temperature	300	[K]	T_s	worst case E-bay temperature
<hr/>				
Demodulation & Uncertain Losses				
eff. data rate	5000	[kbps]	R	50 % of max. data rate
FEC coding	none	[$-$]	n/a	n/a
technical degradation	1	[dB]	L_{i1}	[45]
implementation loss	1	[dB]	L_{i1}	[45]

The free space loss L_s [m^3] in Table E.1 is calculated using the following correlation.

$$L_s = \frac{(4\pi s)^2 \cdot c}{f} \quad (5.3)$$

The signal travel distance s is assumed to be $s = 2000 \text{ m}$ which is in excess of the mission goal described in Section 3.1. In accordance with X-Band communication the frequency f is set to a value of $f = 8.2 \text{ GHz}$. The parameter c represents the speed of light in vacuum. For simplification purposes $c = 3 \cdot 10^9 \frac{\text{m}}{\text{s}}$ is assumed.

Combining the parameters from Table E.1 the link budget is calculated using Equation 5.4. For the simplification of Equation 5.4 the line losses for the rover L_{l1} and lander L_{l2} are expressed as the sum L_l . In the same manner technical degradation and implementation losses are combined to L_i . Atmospheric losses L_a and pointing errors in Equation 5.4 are neglected due to a lack of atmosphere and the utilisation of omnidirectional low gain antennas. Parameter k describes the Boltzmann constant.

$$\frac{E_b}{N_0} = P - L_l + G_R - 10 \cdot \log L_s - L_a + G_L + 10 \cdot \log k - 10 \cdot \log T_s - 10 \cdot \log R - L_i \quad (5.4)$$

Equation 5.4 and the conservative assumptions from Table E.1 results in an energy per bit over noise $\frac{E_b}{N_0} = 10.59 \text{ dB}$. The complete link budget can be found in Table E.2.

Referencing Figure E.1 a Bit Error Rate of 10^{-4} can be achieved in the downlink path, which is considered sufficient for a first assessment. Optionally a FEC code can be implemented in later design phases.

Using the same parameters listed in Table E.1 leads to a $\frac{E_b}{N_0} = 50.56 \text{ dB}$ corresponding to a Bit Error Rate of potentially less than 10^{-6} . Therefore the downlink does not contribute to the design decisions. The complete link budget for the uplink path can be found in Table E.3.

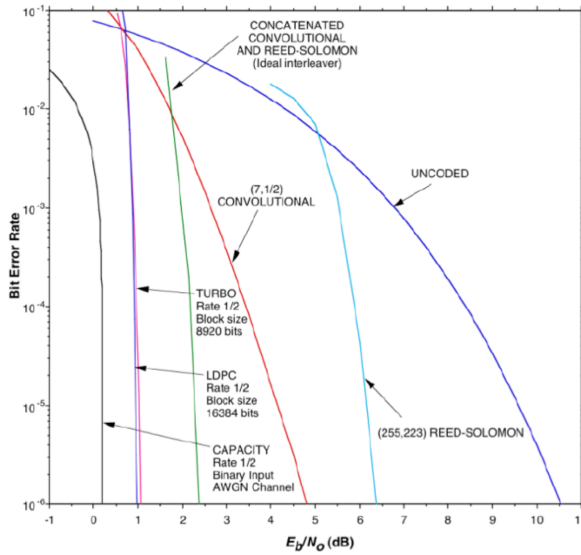


Figure E.1: Bit Error Rate for different FEC codes

Table E.2: Complete link budget for Rover to Lander transmission.

Rover to Lander (R2L) Link Budget (uplink)			
Rover			
Rover transmitter output power	P_R	1	W
	P_R	0	dB
Rover line loss	L_{l1}	0.6	dB
Rover antenna gain	G_R	2	dB
Downlink Path			
Rover antenna pointing loss	n/a	0	dB
polarization loss	L_p	0.3	dB
free space loss	L_s	116.74	dB
atmospheric loss	L_a	0	dB
signal level at Lander	RIP	-115.64	dB
Lander			
Lander LGA pointing loss		0	dB
Lander antenna gain	G_L	1	dB
signal after Lander LGA		-114.64	dB
Lander line loss	L_{l2}	0.6	dB
Lander effective noise temp.	T_s	24.77	dB
Lander signal to noise power density	$\frac{C}{N_0}$	88.58	dB
Data Rate			
data rate	R	5000	kbps
	R	-66.99	dBHz
Total			
System $\frac{E_b}{N_0}$ for L2R link	$\frac{E_b}{N_0}$	21.59	dB
Demodulation			
specified Bit Error Rate	BER	10^{-4}	n/a
FEC coding used		none	
$\frac{E_b}{N_0}$ threshold		9	dB
Uncertain Losses			
technical degradation	L_{i1}	1	dB
implementation loss	L_{i2}	1	dB
Link Margin			
system link margin after uncertain losses	$\frac{E_b}{N_0}$	10.59	dB

Table E.3: Complete link budget for Lander to Rover (L2R) transmission.

Lander to Rover (L2R) Link Budget (downlink)			
Lander			
Lander transmitter output power	P_L	5	W
	P_L	6.99	dB
Lander line loss	L_{l2}	0.6	dB
Lander antenna gain	G_L	1	dB
Uplink Path			
pointing loss	n/a	0	dB
polarization loss	L_p	0.3	dB
free space loss	L_s	116.74	dB
atmospheric loss	L_a	0	dB
signal level at Lander	RIP	109.65	dB
Rover			
Rover LGA pointing loss	n/a	0	dB
Rover antenna gain	G_R	1	dB
signal after Rover LGA		108.65	dB
Rover line loss	L_{l1}	0.6	dB
Rover effective noise temp.	T_s	24.77	dB
Rover signal to noise power density	$\frac{C}{N_0}$	94.57	dB
Data Rate			
data rate	R	2	kbps
	R	33.01	dBHz
Total			
System $\frac{E_b}{N_0}$ for L2R link		61.56	dB
Demodulation			
specified Bit Error Rate	BER	10^{-6}	n/a
FEC coding used		none	
$\frac{E_b}{N_0}$ threshold		11	dB
Uncertain Losses			
technical degradation	L_{i1}	1	dB
implementation loss	L_{i1}	1	dB
Link Margin			
system link margin after uncertain losses	$\frac{E_b}{N_0}$	48.56	dB

E.2 Mission Data Output

The analysis of the mission data concept for memory capacity and transmission times is focuses on the payload camera and hazcams as images require far more data than telemetry or other payload data.

In a first assumption 420 images per day are stored and transmitted. Considering the sensor resolution of 2048×2048 pixels and a bit depth per pixel of 10 bit, a file size of 42 Mbit per image is assumed (camera datasheet in Table H.1).

To calculate the message size in Table E.4, it is assumed that a transmission frame consists of 10264 bits including a payload frame of maximum 8840 bits [46].

Table E.4: Comparison of transmission times per image (message frame bits included)

File Type	Compression	File Size	Message Size	Data Rate	Tx t per File
image	none	42 Mbit	48.77 Mbit	5 Mbit	8.12 s
image	HIREW	23.52 Mbit	27.31 Mbit	5 Mbit	5.45 s

Table E.5: Transmission time and total data output per mission day

File per tal	Compression	File Size	Total Data	Tx time
420	none	42 Mbit	2.21 GB	56.9 Min.
420	HIREW	23.52 Mbit	1.22 GB	38.23 Min.

The HIREW compression algorithm is suggested for the mission considering a high average compression of 0.56 % and a high compression speed of 123 Mbit/s for grayscale and 104.4 Mbit/s for RGB image files [47].

F Thermal Controls System

F.1 Results

Table F.1: Temperature results in K of thermal analysis, *with out* margin .

Components	Hot Case	Cold Case	Charging	Communication	Analyse
RTG	415	391	402	407	401
Electric Bay	301	268	293	313	28
Drill	283	256	267	271	328
Camera	327	249	256	257	256
Chassis	268	230	245	251	246
Steer Engine	296	249	260	262	261
Drive Engine	344	251	262	262	262

Table F.2: Temperature results in K of thermal analysis, *with* margin .

Components	Hot Case	Cold Case	Charging	Communication	Analyse
Margin	+15 K	-15 K	+15 K	+15 K	+15 K
RTG	430	376	417	422	416
Electric Bay	316	253 ¹⁾	308	328 ¹⁾	296
Drill	298	241	282	286	343
Camera	342	234	271	272	271
Chassis	283	215	260	266	261
Steering Engine	311	234	275	277	276
Drive Engine	359	236	277	277	277

¹⁾ Exceeding transmitter temperature limits.

F.2 Heat energy eqilibrium

The follwing equiations describe each node of the thermal network. The input values were tanken from EPS, Subsection F.3, Subsection F.4, Subsection F.5 respectively.

Subscript for eqilibrium:

Bay	Electrical Bay	D	Drill
Bo	Bogie	E,D	Drive Engine
Cam	Camera	E,S	Steer Engine
C	Chassis	WF	Wheel Fork

RTG:

$$\begin{aligned}
 0 = & \dot{Q}_{RTG} + CON_1 \cdot (T_{Bay} - T_{RTG}) + CON_2 \cdot (T_C - T_{RTG}) + \\
 & + CON_5 \cdot (T_D - T_{RTG}) + CON_9 \cdot (T_{E,S} - T_{RTG}) \\
 & + CON_{12} \cdot (T_{E,D} - T_{RTG}) - \epsilon_{RTG} \cdot \sigma_b \cdot S_{RTG} \cdot T_{RTG}^4
 \end{aligned} \tag{5.5}$$

Electric Bay:

$$\begin{aligned}
 0 = & \dot{Q}_{Bay} + CON_1 \cdot (T_{RTG} - T_{Bay}) + (CON_3 + n_{S2} \cdot CON_{S2}) \cdot (T_C - T_{Bay}) - \\
 & - \epsilon_{Bay} \cdot \sigma_b \cdot S_{Bay} \cdot T_{Bay}^4
 \end{aligned} \tag{5.6}$$

with:

$$\dot{Q}_{Bay} = \dot{Q}_{OBC} + \dot{Q}_{Tranceiver} + \dot{Q}_{Receiver} + \dot{Q}_{PCDU} \tag{5.7}$$

Drill & Analyser:

$$0 = \dot{Q}_D + CON_4 \cdot (T_C - T_D) + CON_5 \cdot (T_{RTG} - T_D) \tag{5.8}$$

Camera:

$$\begin{aligned}
 0 = & \dot{Q}_{Cam} + \dot{Q}_{RHU} + CON_6 \cdot (T_C - T_{Cam}) + \\
 & + (CON_{14} + n_{S1} \cdot CON_{S1}) \cdot (T_{Rad} - T_{Cam}) - \\
 & - \epsilon_{Cam} \cdot \sigma_b \cdot S_{Cam} \cdot T_{Cam}^4
 \end{aligned} \tag{5.9}$$

Radiator:

$$0 = (CON_{14} + n_{S1} \cdot CON_{S1}) \cdot (T_{Cam} - T_{Rad}) - \epsilon_{Rad} \cdot \sigma_b \cdot S_{Rad} \cdot T_{Rad}^4 \tag{5.10}$$

Chassis:

$$\begin{aligned}
 0 = & \dot{Q}_{Radar} + \dot{Q}_{Hazcam} + \dot{Q}_{Analyser} + \dot{Q}_{IMUs} + \\
 & + CON_2 \cdot (T_{RTG} - T_C) + (CON_3 + n_{S2} \cdot CON_{S2}) \cdot (T_{Bay} - T_C) + \\
 & + CON_4 \cdot (T_{Drill} - T_C) + CON_6 \cdot (T_{Cam} - T_C) + CON_7 \cdot (T_{Node1} - T_C) + \\
 & + \alpha_C \cdot [S_0 \cdot (1 + \rho_E) \cdot (S_{Ch1} \cdot \varphi_1 + S_{Ch2} \cdot \varphi_2) + \epsilon_E \cdot \sigma_b \cdot S_{Ch3} \cdot T_{Surface}^4] + \\
 & + \epsilon_{Bay} \cdot \sigma_b \cdot S_{Bay} \cdot T_{Bay}^4 - \frac{1}{2} \cdot \epsilon_{Bo} \cdot \sigma_b \cdot S_{Bo} \cdot \left(\frac{T_C}{2} + \frac{T_{Node1}}{2} \right)^4 - \epsilon_C \cdot \sigma_b \cdot S_C \cdot T_C^4
 \end{aligned} \tag{5.11}$$

Steer Engine:

$$0 = 4 \cdot [\dot{Q}_{E,S} + CON_8 \cdot (T_{Node1} - T_{E,S}) + \\ + CON_9 \cdot (T_{RTG} - T_{E,S}) - \epsilon_{E,S} \cdot \sigma_b \cdot S_{E,S} \cdot T_{E,S}^4] \quad (5.12)$$

Distribution Node 1:

$$0 = 4 \cdot [CON_7 \cdot (T_C - T_{Node1}) + CON_8 \cdot (T_{E,S} - T_{Node1}) + \\ + CON_10 \cdot (T_{Node2} - T_{Node1}) - \\ - \frac{1}{2} \cdot \epsilon_{Bo} \cdot \sigma_b \cdot S_{Bo} \cdot \left(\frac{T_C}{2} + \frac{T_{Node1}}{2} \right)^4 - \\ - \frac{1}{2} \cdot \epsilon_{WF} \cdot \sigma_b \cdot S_{WF} \cdot \left(\frac{T_{Node1}}{2} + \frac{T_{Node2}}{2} \right)^4 - \\ - \epsilon_{E,S} \cdot \sigma_b \cdot S_{E,S} \cdot T_{E,S}^4] \quad (5.13)$$

Drive Engine:

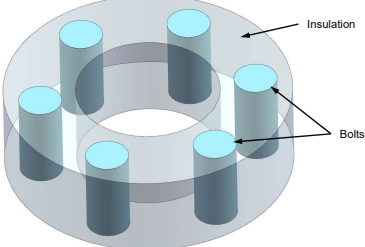
$$0 = 4 \cdot [\dot{Q}_{E,D} + (CON_{11} + n_{S3} \cdot CON_{S3}) \cdot (T_{Node2} - T_{E,D}) + \\ + CON_{12} \cdot (T_{RTG} - T_{E,D}) - \epsilon_{E,D} \cdot \sigma_b \cdot S_{E,D} \cdot T_{E,D}^4] \quad (5.14)$$

Distribution Node 2:

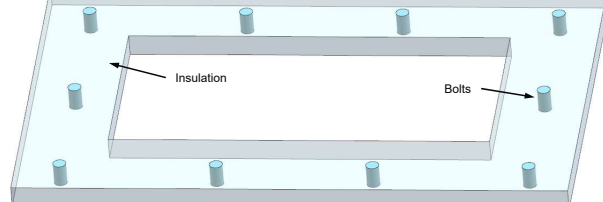
$$0 = 4 \cdot [CON_{10} \cdot (T_{Node1} - T_{Node2}) + CON_{13} \cdot (T_{Ground} - T_{Node2}) + \\ + (CON_{11} + n_{S3} \cdot CON_{S3}) \cdot (T_{E,D} - T_{Node2}) + \\ - \frac{1}{2} \cdot \epsilon_{WF} \cdot \sigma_b \cdot S_{WF} \cdot \left(\frac{T_{Node1}}{2} + \frac{T_{Node2}}{2} \right)^4 - \\ - \epsilon_{E,D} \cdot \sigma_b \cdot S_{E,D} \cdot T_{E,D}^4] \quad (5.15)$$

F.3 Heat conductance

Table F.3: Definition of heat conductance C between the nodes according to Figure 4.10.

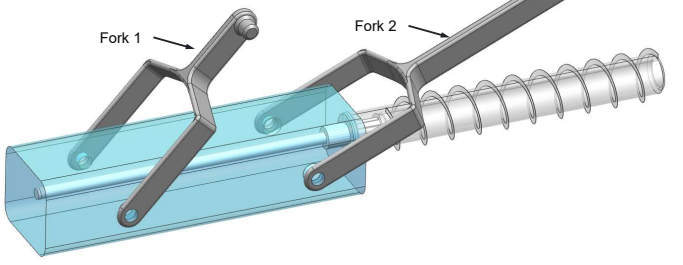
Name	Linked Components	Geometry
Linkage	RTG \leftrightarrow Chassis	
	$CON_2 = CON_I + n_B \cdot CON_B$	
	$CON_2 = 1.50 \cdot 10^{-1} \frac{W}{K}$	

Part	Cross section	Thickness	Material	Amount
Insulation	$S_I = 3'770 \text{ mm}^2$	$t_I = 12 \text{ mm}$	Aerogel	1
Bolts, M6	$S_B = 28.3 \text{ mm}^2$	$t_B = 12 \text{ mm}$	Titan	10

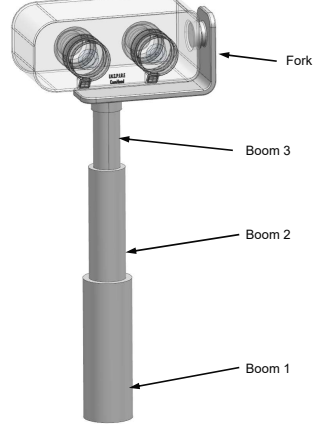
Name	Linked Components	Geometry
Linkage	EBay \leftrightarrow Chassis	
	$CON_3 = CON_I + n_B \cdot CON_B$	
	$CON_3 = 4.20 \cdot 10^{-1} \frac{W}{K}$	

Part	Cross section	Thickness	Material	Amount
Insulation	$S_I = 27'120 \text{ mm}^2$	$t_I = 8 \text{ mm}$	Aerogel	1
Bolts, M6	$S_B = 28.3 \text{ mm}^2$	$t_B = 8 \text{ mm}$	Titan	10

Table F.4: Definition of heat conductance $CON = \frac{1}{R}$ between the nodes according to Figure 4.10.

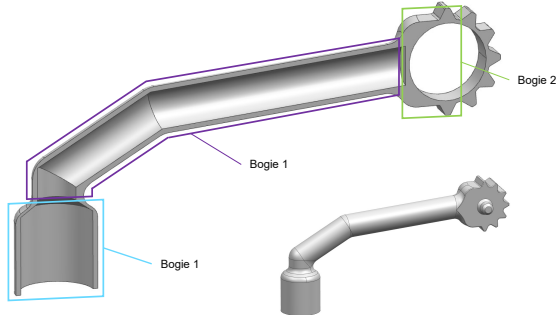
Name	Linked Components	Geometry
Linkage	Drill \leftrightarrow Chassis	

Part	Cross section	Length	Material	Amount
Fork 1	$S_{F1} = 40 \text{ mm}^2$	$l_{F1} = 90$	Aluminium	1
Fork 1	$S_{F2} = 40 \text{ mm}^2$	$l_{F2} = 150$	Aluminium	1

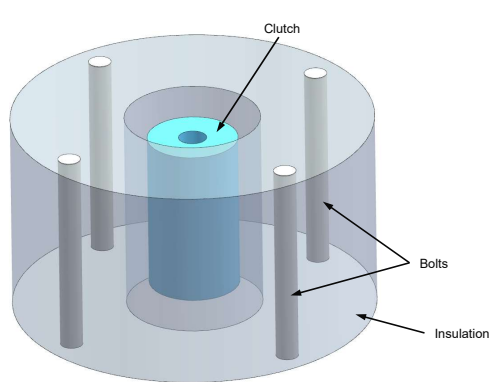
Name	Linked Components	Geometry
Telescope	Camera \leftrightarrow Chassis	

Part	Cross section	Length	Material	Amount
Boom 1	$S_{B1} = 181 \text{ mm}^2$	$l_{B1} = 116 \text{ mm}$	Aluminium	1
Boom 2	$S_{B2} = 134 \text{ mm}^2$	$l_{B2} = 95 \text{ mm}$	Aluminium	1
Boom 3	$S_{B3} = 97 \text{ mm}^2$	$l_{B3} = 60 \text{ mm}$	Aluminium	1
Fork	$S_F = 200 \text{ mm}^2$	$l_F = 170 \text{ mm}$	Aluminium	1

Table F.5: Definition of heat conductance $CON = \frac{1}{R}$ between the nodes according to Figure 4.10.

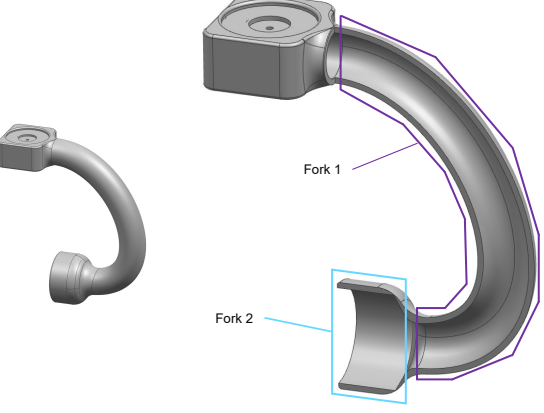
Name	Linked Components	Geometry
Suspension	Chassis \leftrightarrow Node₁	 $CON_7 = \left(\frac{1}{CON_{B1}} + \frac{1}{CON_{B2}} + \frac{1}{CON_{B3}} \right)^{-1}$ $CON_7 = 1.30 \cdot 10^{-1} \frac{\text{W}}{\text{K}}$

Part	Cross section	Length	Material	Amount
Bogie 1	$S_{B1} = 275 \text{ mm}^2$	$t_{B1} = 20 \text{ mm}$	Aluminium	1
Bogie 2	$S_{B2} = 113 \text{ mm}^2$	$t_{B2} = 162 \text{ mm}$	Aluminium	1
Bogie 3	$S_{B3} = 201 \text{ mm}^2$	$t_{B3} = 37 \text{ mm}$	Aluminium	1

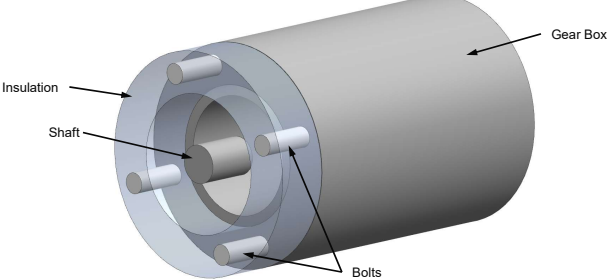
Name	Linked Components	Geometry
Mounting	Steer Engine \leftrightarrow Node₁	 $CON_8 = CON_C + CON_I + n_B \cdot CON_B$ $CON_8 = 7.62 \cdot 10^{-1} \frac{\text{W}}{\text{K}}$

Part	Cross section	Thickness	Material	Amount
Clutch	$S_C = 45.4 \text{ mm}^2$	$t_C = 14 \text{ mm}$	Aluminium	1
Insulation	$S_I = 691 \text{ mm}^2$	$t_I = 18 \text{ mm}$	Aerogel	1
Bolts	$S_B = 3.14 \text{ mm}^2$	$t_B = 18 \text{ mm}$	Steel	4

Table F.6: Definition of heat conductance $CON = \frac{1}{R}$ between the nodes according to Figure 4.10.

Name	Linked Components	Geometry
Wheel Fork	Node₁ ↔ Node₂	

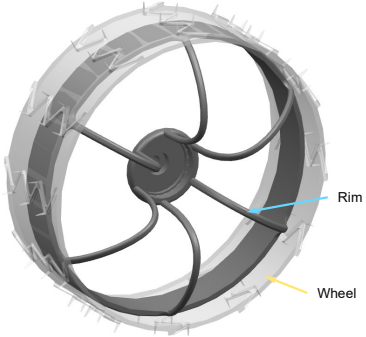
Part	Cross section	Length	Material	Amount
Fork 1	$S_{F1} = 113 \text{ mm}^2$	$l_{F1} = 160$	Aluminium	1
Fork 1	$S_{F2} = 226 \text{ mm}^2$	$l_{F2} = 20$	Aluminium	1

Name	Linked Components	Geometry
Mounting	Drive Engine ↔ Node₂	

Part	Cross section	Thickness	Material	Amount
Gear Box	$S_G = 566 \text{ mm}^2$	$t_G = 43.1 \text{ mm}$	Steel	1
Shaft	$S_S = 23.8 \text{ mm}^2$	$t_S = 10 \text{ mm}$	Steel	1
Insulation	$S_I = 490 \text{ mm}^2$	$t_I = 10 \text{ mm}$	Aerogel	1
Bolts, M3	$S_B = 7.07 \text{ mm}^2$	$t_B = 10 \text{ mm}$	Titan	4

F. THERMAL CONTROLS SYSTEM

Table F.7: Definition of heat conductance $CON = \frac{1}{R}$ between the nodes according to Figure 4.10.

Name	Linked Components	Geometry		
Rim	Node₂ ↔ Ground			
	$CON_{13} = 1.06 \cdot 10^{-1} \frac{\text{W}}{\text{K}}$			
Part	Cross section	Length	Material	Amount
Rim	$S_R = 8 \text{ mm}^2$	$l_r = 100 \text{ mm}$	Aluminium	6

Note: It was assumed that the wheel temperature equals the surface temperature because of the thin rims and resulting low heat conduction.

F.4 Heat switch

The characteristic of the switch conductance depends on the mean temperature T_M , shown by measurements in cite . As this temperature won't be calculated in the analysis, the corresponding component temperature T_C shall be used. In order to describe the characteristic, it was divided in three sections, Figure F.1. The temperature where the disk decouples is $T_{toggle} = 108K$ and not applicable for the current application. By reducing the height, the toggle temperature can be increased and the characteristic can be shifted to higher temperatures ("to the right"). It was assumed that the gradients of section 2 and 3 as well as the temperature range of section 2 keep constant. The axis interception is a function the toggle temperature ($a_2 = f(\Delta T_{toggle})$, $\Delta T_{Toggle} = T_{new} - T_{old}|_{toggle}$). The used toggle temperature are listed in autoref

Table F.8: Toggle temperature and amount of bi-metallic heat switch.

Heat switch name	Linked Components	Temperature	Amount
CON_{S1}	Camera ↔ Radiator	-28 °C	$n_{S1} = 4$
CON_{S2}	EBay ↔ Chassis	-5 °C	$n_{S2} = 2$
CON_{S3}	Drive Engine ↔ Node ₂	-20 °C	$n_{S3} = 1$ (in total 4)

Table F.9: Sections and range of the switch characteristic.

Section	Temperature range	Heat conductance $CON_S = \frac{1}{R_t}$
1	$T_{toggle} > T_C$	$CON_S = 16.4 \cdot 10^{-3} \frac{\text{W}}{\text{m}^2\text{K}} = const.$
2	$T_{toggle} \leq T_C < T_1$	$CON_S(T_C) = a_{1.1} \cdot T_C + a_{1.2}$ $a_{1.1} = +1.272 \cdot 10^{-3} \frac{\text{W}}{\text{m}^2\text{K}^2}$ $a_{1.2} = -1.272 \cdot 10^{-3} \frac{\text{W}}{\text{m}^2\text{K}^2} \cdot \Delta T_{Toggle} - 0.117 \frac{\text{W}}{\text{m}^2\text{K}}$
3	$T_C > T_1$	$CON_S(T_C) = a_{2.1} \cdot T_C + a_{2.2}$ $a_{2.1} = +333 \cdot 10^{-6} \frac{\text{W}}{\text{m}^2\text{K}^2}$ $a_{2.2} = -333 \cdot 10^{-6} \frac{\text{W}}{\text{m}^2\text{K}^2} \cdot \Delta T_{Toggle} - 28.3 \cdot 10^{-3} \frac{\text{W}}{\text{m}^2\text{K}}$

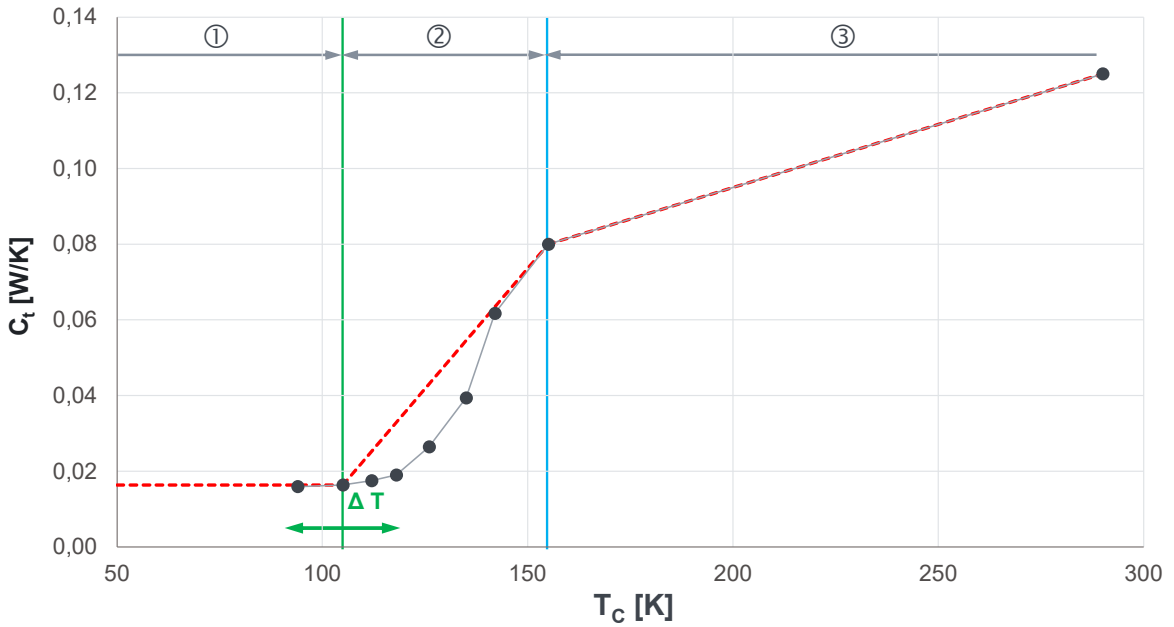


Figure F.1: Conductance characteristic of heat switch divided in sections.

F.5 Rover absorptivity

The rover position relative to the direct sun radiation is given by the ecliptic longitude λ_R and latitude δ_R angle, where the axis x_E points always to the sun, Figure F.2b. The amount of solar radiation S_0 absorbed by the rover surfaces depends on the sun altitude and can be determined by the view factor φ , see Figure F.2a. The view factors during the eclipse are set to zero.

$$\begin{aligned} \text{View Factor 1, horizontal surface: } & \varphi_1 = \cos(\lambda_R) \cdot \cos(\delta_R) \\ \text{View Factor 2, vertical surface: } & \varphi_2 = \cos(90^\circ - \lambda_R) \cdot \cos(\delta_R) \end{aligned}$$

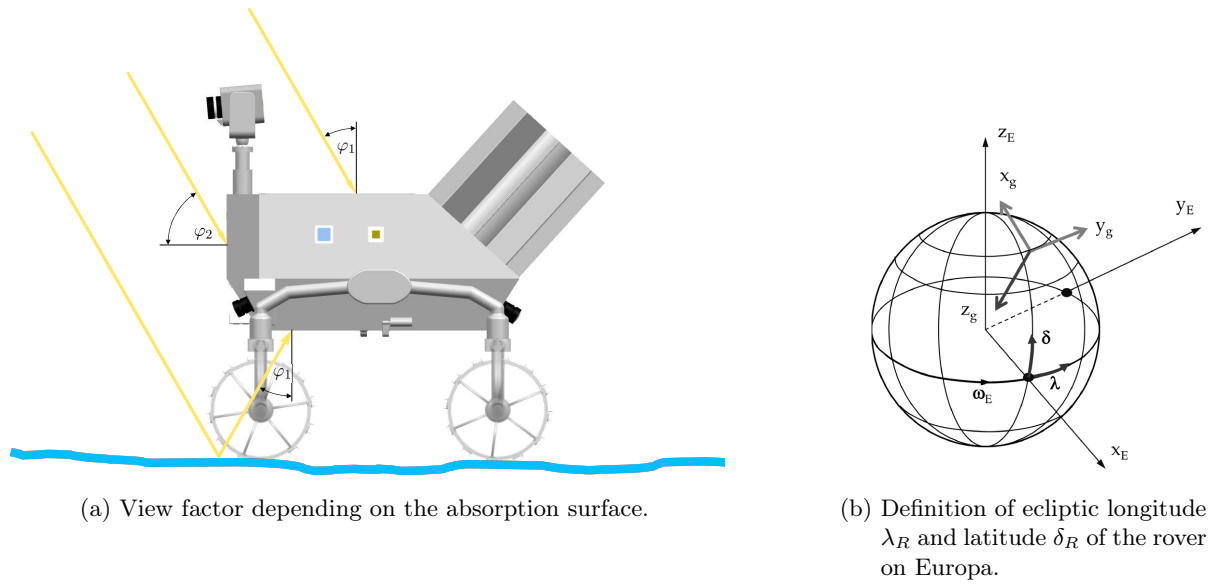


Figure F.2: Bi-metallic heat switch [37].

F.6 Input Values

Table F.10: Temperatur limits of the rover components.

Component	Temperature limits in [°C]	
	min.	max.
OBC	-55	70
Transmitter	-10	50
Receiver	-30	70
PCDU	-40	60
Battery	-20	60
Camera	-40	70
Objektive	-40	71
Steering Engine	-30	100
Drive Engine	-40	100
Drive Gear	-40	100

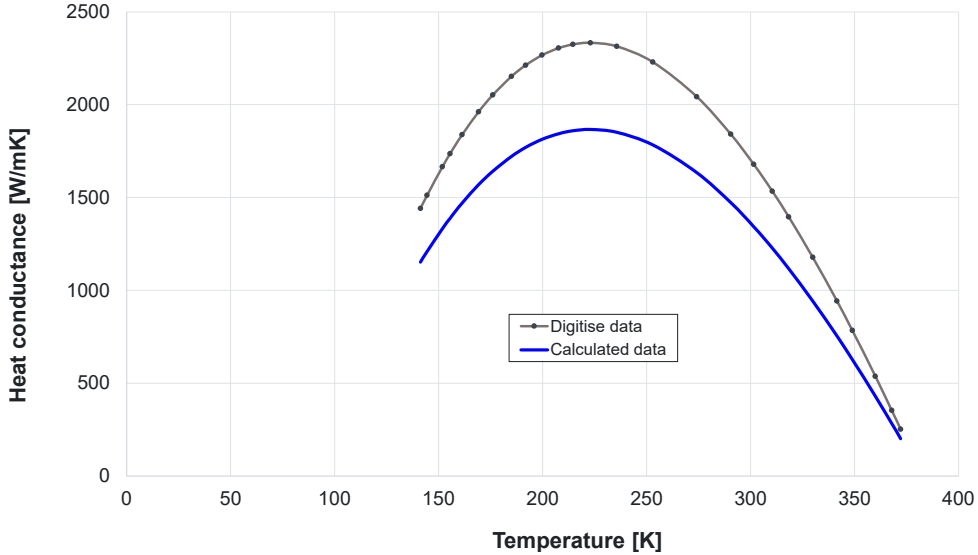


Figure F.3: Digitalised [34] and calculated heat conduction in comparison.

The characteristic of the *LyNX®* conduction was approximated with following function,

$$\lambda(T) = \left(1.76 \cdot 10^{-4} \frac{\text{W}}{\text{mK}^4} \cdot T^3 - 2.37 \cdot 10^{-1} \frac{\text{W}}{\text{mK}^3} \cdot T^2 + 79.5 \frac{\text{W}}{\text{mK}^2} \cdot T - 5.55 \cdot 10^3 \frac{\text{W}}{\text{mK}} \right) \cdot f_r \quad (5.16)$$

with the reduction factor $f_r=0.8$.

Table F.11: Dimensions of the thermal straps *LyNX®*.

Linked Components	Cross section	Length ¹⁾
EBay \leftrightarrow RTG	42 mm ²	230 mm
Drill \leftrightarrow RTG	10 mm ²	345 mm
Steer Engine \leftrightarrow RTG	36 mm ²	644 mm
Drive Engine \leftrightarrow RTG	42 mm ²	897 mm

¹⁾ Due to uncertainties the length was increased about 15%.

The Europa surface temperature varies at the equator between $T_{e,min} = 80$ K and $T_{e,max} = 130$ K, depending on the sun inclination. The temperature at the pole is $T_{Pole} = 50$ K [15]. It was assumed that the surface temperature depends on the sun altitude. A trigonometrical interpolation was defined as follows.

$$T_{Surface}(\lambda, \delta) = T_{Pole} + \cos(\delta) \cdot [(T_{e,min} + \cos(\lambda) \cdot (T_{e,max} - T_{e,min})) - T_{Pole}]$$

For λ and δ see Subsection F.5.

F. THERMAL CONTROLS SYSTEM

Table F.12: Minimum and maximum of surface emissivity and absorptivity values [38].

Surface finishing	Emissivity [-]		Absorptivity [-]	
	min.	max.	min.	max.
Aluminium, polished	0.04	0.06	0.16	0.24
Aluminium, sandblasted	0.16	0.242	0.36	0.44
White paint	0.8	0.9	0.2	0.5

Table F.13: Heat conductivity in $\frac{\text{W}}{\text{mK}}$

Material	Nominal	Used	Source
Aerogel	0.002 - 0.05	0.05	[36]
Aluminium ¹⁾	110 - 220	220	[48] [49] [16]
Steel ¹⁾	15 - 43	45	[50] [51]
Titan	7.1	7.1	[52] [53]

¹⁾ Depends on the alloying component, a conservative value was chosen.

Table F.14: Radiation surface and finishing of components.

Part	Surface [m^2]	Finishing	Note
Chassis - top/bottom	$S_{Ch1} = 0.086$	white paint	for albedo
Chassis - side	$S_{Ch2} = 0.081$	white paint	for albedo
Chassis - total	$S_{Ch3} = 0.423$	white paint	for emissivity
RTG	$S_{RTG} = 0.086$	white paint	konstant emissivity of 0.9
Electric Bay	$S_{Bay} = 0.146$	AL, sand blastet	
Camera - housing	$S_{Cam} = 0.027$	AL, sand blastet	
Camera - radiator	$S_{Rad} = 0.066$	white paint	
Steer Engine	$S_{E,S} = 0.002$	white paint	
Drive Engine	$S_{E,D} = 0.003$	white paint	
Bogie	$S_B = 0.018$	white paint	
Wheel Fork	$S_F = 0.008$	white paint	

The cross sections were taken from the CAD model.

G Radiation

In this chapter, detailed calculations are performed on which Section 4.6 is based on. All calculations and figures in Section G are performed with SPENVIS unless otherwise stated. In order to simulate the radiation on Europa an orbit around Jupiter is simulated with the orbit parameters of Europa with a total mission duration of 30 days. The chosen parameters were an perijove altitude of 664,862 km, an apojove altitude of 676,938 km, and an inclination of 0.47°.

G.1 Jupiters Radiation Environment

In order to compare the radiation environment around Jupiter and the radiation environment around Earth the following trapped radiation models were used: for Jupiter the D&G83+Salammbo proton model and D&G83+GIRE+SalammboE electron model was used; for Earth the AP-8 proton model and the AE-8 electron model was used.

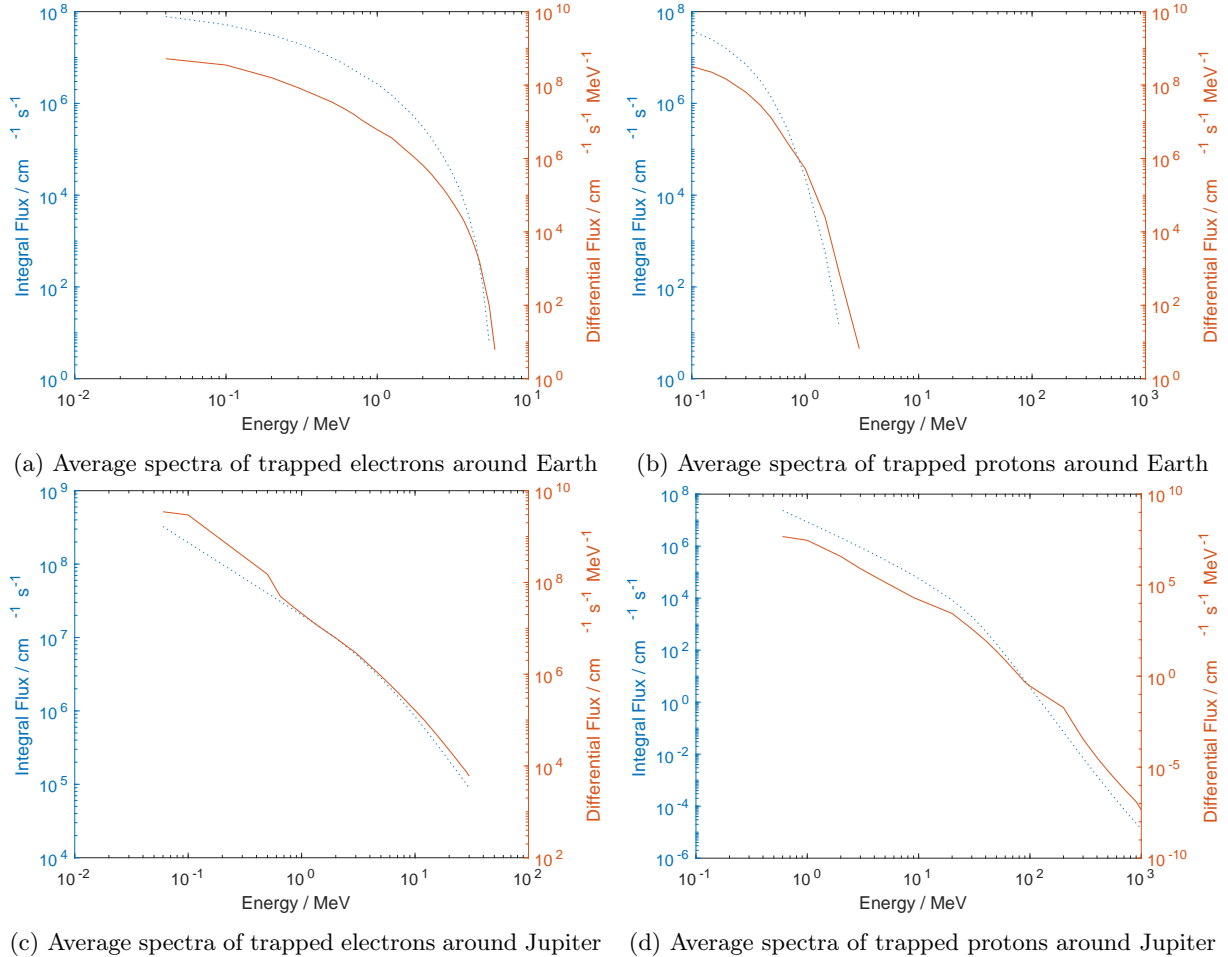


Figure G.1: Average trapped proton and electron fluxes on an orbit around earth at 25,000 km, through the outer Van Allen radiation belt, and on Europa's orbit around Jupiter.

G.2 Radiation Exposures

In order to simulate the TID for different radiation protections the Geant4 tool Multi-Layered Shielding Simulation (MULASSIS) is used. As target material silicon is selected with a thickness of $1 \mu\text{m}$. As shape a planar slap is selected because of the ice ground on one side of the rover.

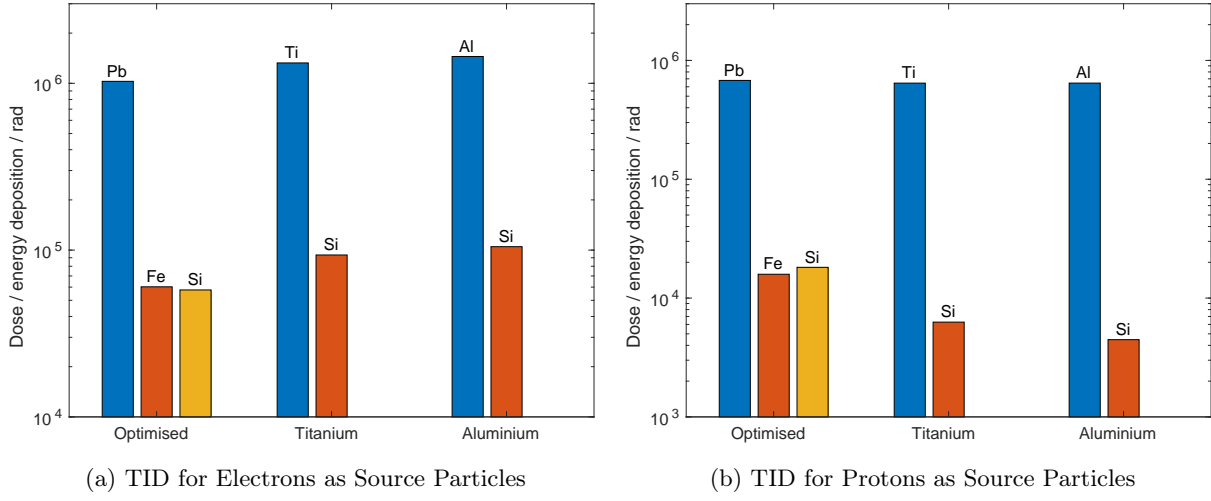


Figure G.2: TID of aluminium, titanium, and the optimised radiation structure shown in Table 4.6 with a weight target of all three structures of 0.5 g/cm^2 over 30 days of exposure on Europa.

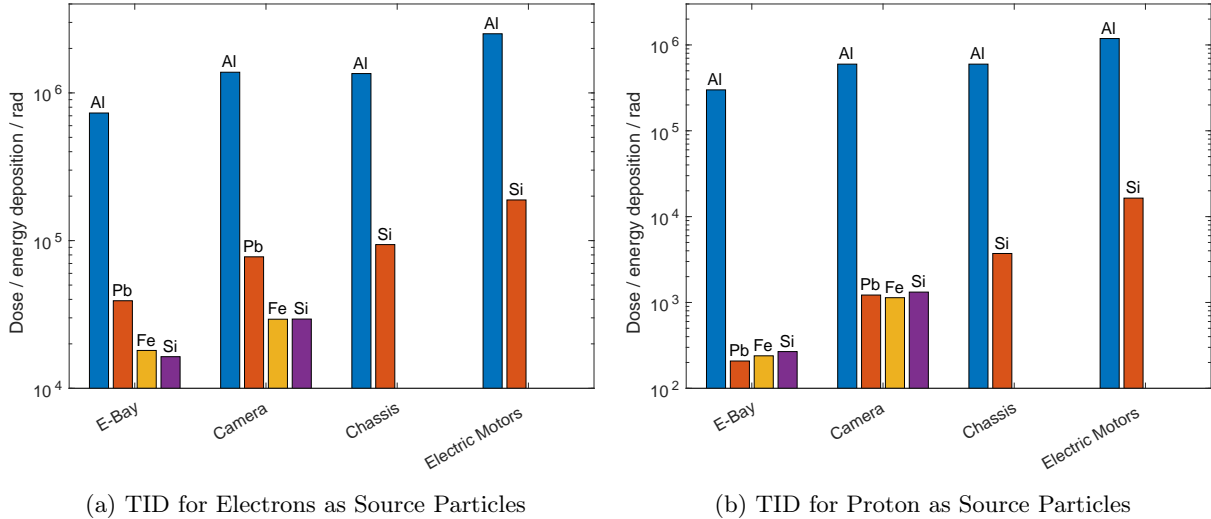


Figure G.3: TID for different compartments as seen in Figure 4.11. The E-Bay is shielded by 4 mm aluminium, 0.415 mm lead, and 0.033 mm iron; the camera compartment by 2 mm aluminium, 0.415 mm lead, and 0.033 mm iron; the chassis by 2 mm aluminium; the electric motors by 1 mm aluminium.

Table G.1: Used components and the respective radiation tolerance and location

Components	Rated TID	Exposed TID	Location
BLDC Motors	-	< 205	locomotion housing
Stepper Motors	100 000	< 205	locomotion housing
Harness	-	< 98	chassis
Stereo Vision Cams	40	< 31	camera housing
OBC	1 000	< 17	E-Bay
PCDU	20	< 17	E-Bay
Transmitter	20	< 17	E-Bay
Receiver	20	< 17	E-Bay
Battery	20	< 17	E-Bay
Housekeeping Board	≈ 20	< 17	E-Bay
IMU	≈ 20	< 17	E-Bay
Multiplexer	≈ 20	< 17	E-Bay
Ground Radar	≈ 20	< 17	E-Bay
Sun Sensor	10 000	2 000	outside rover
Camera Lenses	10 000	2 000	outside rover

G.3 Improvements

All simulations of the improvements introduced in Subsection 4.6.3 are performed in the same way as in Subsection G.2.

In Figure G.4, the TID over 30 days within the E-Bay is shown with only the aluminium structure. If all components with a radiation resistance under 43.27 krad are shielded individually, the additional shielding structure around the E-Bay can be removed and the aluminium structure would be sufficient.

The aluminium structure would also be sufficient if a layer of 1 cm of water mined in-situ would be used as shielding which is present in Figure G.5.

Both improvements would save the mass of the lead and iron shielding for the optimised shielding of 897.2 g.

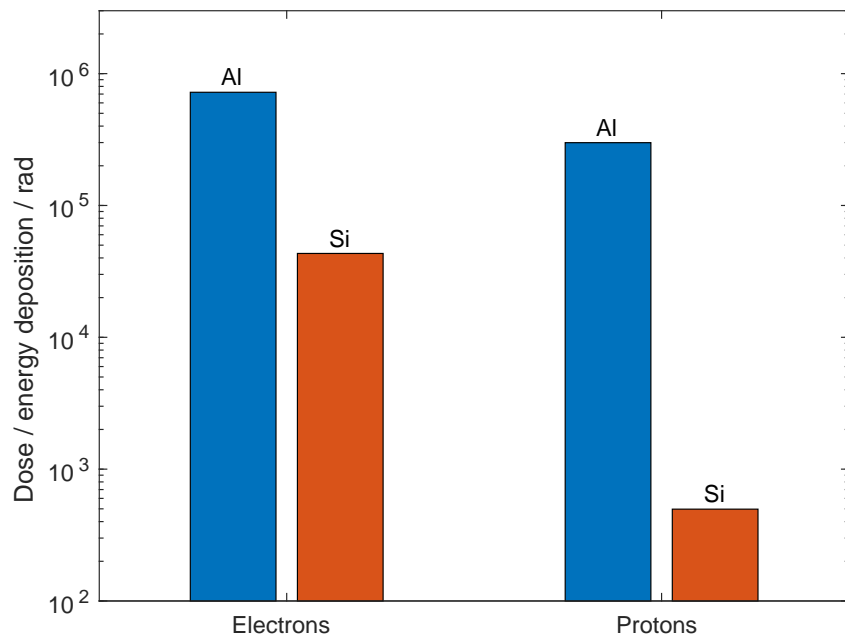


Figure G.4: TID with 4 mm Al shielding over a mission duration of 30 days

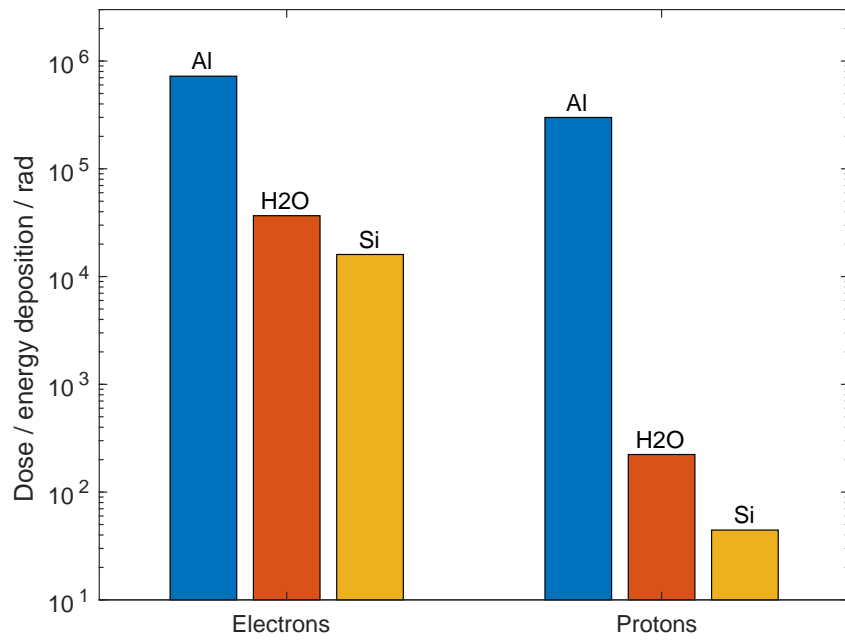


Figure G.5: TID with 4 mm Al shielding and 1 cm of Water over a mission duration of 30 days

H Digital Appendix

Table H.1: Digital Appendix

Name	Path	Type	Size
TCS Analysis final	300 Thermal	Excelsheet with Macros, *.xlsm	189 kB
Comms & C&DH Datasheets	600_C&DH_Communication	*.pdf	42.5 MB
Comms & C&DH Trade Offs	600_C&DH_Communication	*.png	479 kB
Locomotion MMP Deflection	200 Locomotion	Excelsheet with Data, *.xlsx	101 kB
Locomotion Motor wheels EC32flat	200 Locomotion	PDF Datasheet, *.pdf	101 kB
Locomotion PlanetaryGear Wheels	200 Locomotion	PDF Datasheet, *.pdf	180 kB
Locomotion StepperMotors physpace	200 Locomotion	PDF Datasheet, *.pdf	1610 kB
Locomotion IMU Vectornav VN-110	200 Locomotion	PDF Datasheet, *.pdf	3718 kB
MMP	200 Locomotion	Matlab File, *.m	3 kB
ResistanceHeavyClay	200 Locomotion	Matlab File, *.m	4 kB
ResistanceSnow	200 Locomotion	Matlab File, *.m	4 kB
Sinkage HeavyClay	200 Locomotion	Matlab File, *.m	3 kB
Sinkage Snow	200 Locomotion	Matlab File, *.m	3 kB
SoilThrustHeavyClay	200 Locomotion	Matlab File, *.m	4 kB
SoilThrustSnow	200 Locomotion	Matlab File, *.m	4 kB
SinkageSnow	200 Locomotion	Excelsheet with Data, *.xlsx	4 kB
SinkageClay	200 Locomotion	Excelsheet with Data, *.xlsx	4 kB
Torque and Power	200 Locomotion	Excelsheet with Data, *.xlsx	11 kB
WheelDimensionsV3 reduced	200 Locomotion	Excelsheet with Data, *.xlsx	11 kB
WheelDimensionsV3 groß	200 Locomotion	Excelsheet with Data, *.xlsx	12 kB
Tradeoff Locomotion	200 Locomotion	Excelsheet with Data, *.xlsx	475 kB
Lens Assembly	700 Payload	PDF Datasheet, *.pdf	353 kB
RadHard Lenses Schott	700 Payload	PDF Datasheet, *.pdf	338 kB
PowerLED	700 Payload	PDF Datasheet, *.pdf	843 kB
SpaceGradeCameraCMOS	700 Payload	PDF Datasheet, *.pdf	869 kB
SunSensorSpaceGradeMAUS	700 Payload	PDF Datasheet, *.pdf	487 kB